JAERI-Tech
96-024

JAPAN-AUSTRALIA CO-OPERATIVE PROGRAM ON RESEARCH AND DEVELOPMENT OF TECHNOLOGY FOR THE MANAGEMENT OF HIGH LEVEL RADIOACTIVE WASTES : PHASE II (1990-1995)

May 1996

(Eds.) Tsunetaka BANBA and Kaye P. HART*

日本原子力研究所
Japan Atomic Energy Research Institute

本レポートは，日本原子力研究所が不定期に公刊している研究報告書です。
入手の問合わせは，日本原子力研究所技術情報部情報資料課（〒319-11 茨城県那珂郡東海村）あて，お申し越しください。なお，このほかに財団法人原子力弘済会資料センター（〒319-11 茨城県那珂郡東海村日本原子力研究所内）で複写による実費頒布をおこなっております。

This report is issued irregularly.
Inquiries about availability of the reports should be addressed to Information Division, Department of Technical Information, Japan Atomic Energy Research Institute, Tokai-mura, Naka-gun, Ibaraki-ken 319-11, Japan.

編集兼発行　日本原子力研究所
印　　刷　いばらき印刷㈱

JAERI-Tech 96-024

Japan-Australia Co-operative Program on Research and Development of Technology for the Management of High Level Radioactive Wastes: Phase II (1990-1995)

(Eds.) Tsunetaka BANBA and Kaye P. HART*

Department of Environmental Safety Research
Tokai Research Establishment
Japan Atomic Energy Research Institute
Tokai-mura, Naka-gun, Ibaraki-ken

(Received May 1, 1996)

The first five-year phase (Phase I) of this Co-operative Program commenced in 1985 as a consequence of technical and diplomatic discussions in the early 1980s. During Phase I effective mechanisms of information transfer were established through personnel exchanges between JAERI and ANSTO, and a number of technical workshops. At the end of Phase I it was strongly recommended that the Program should be extended into a second five-year period from 1990 to 1995, designated as Phase II. The aims of the Phase II Program were (a) studies on Cm-doping of Synroc containing simulated PW-4b wastes; (b) joint research on the use of Synroc to immobilise the long-lived, transuranic elements; and (c) studies on the behaviour of Synroc under repository conditions.

The major activities associated with the Co-operative Program were the preparation, characterisation and subsequent testing of both Cm-doped Synroc containing PW-4b simulated waste and Cm-doped single-phase zirconolite and perovskite, and the initiation of studies on naturally-occurring zirconolites to study the long-term durability of this mineral phase over geological time. The preparation of the Cm-doped samples was carried out in JAERI's WASTEF facility at Tokai, with technical

---

This report summarizes the results obtained in the second five-year phase (Phase II from 1990 to 1995) of Japan-Australia co-operative program on research and development of technology for the management of high-level radioactive wastes.

* Environmental Science Program, Australian Nuclear Science and Technology Organisation; New Illawarra Road, Lucas Heights, NSW, Australia

information and assistance provided by ANSTO where necessary. The experiments were designed to induce accelerated radiation damage in Synroc samples that would correspond to periods of Synroc storage of up to 100,000 years. The results, described in greater detail in this report, are of considerable importance in evaluating the potential of the Synroc process as a means of dealing with HLW waste streams and represent a significant contribution to the understanding of the ability of Synroc to immobilise HLW elements. In addition, JAERI and ANSTO each conducted a number of parallel, related investigations plus any work required to solve problems that resulted from the main study on the Cm-doped Synroc.

Overall the Phase II Co-operative Program has continued the excellent co-operative working relationship between the staff at the two institutions, and provided a better understanding of the potential advantages and limitations of Synroc as a second generation waste form. The work has shown the need for additional studies to be carried out on the effect of the levels of Cm-doping on the Cm leach rate, extension of natural analogue studies to define the geological conditions under which zirconolite is stable and development of models to provide long-term predictions of releases of HLW elements from Synroc under a range of repository conditions.

It is strongly recommended that the program carried out in Phase II of the Co-operative Agreement be extended for a further three years to allow additional information on the above areas to be collected and reported in a document providing an overview of the Cooperative Program and recommendations on HLW management strategies.

Keywords: High Level Radioactive Wastes, Management, Japan-Australia Co-operative Program, Phase II, Synroc

高レベル放射性廃棄物処理処分技術の研究開発における日本とオーストラリアの研究協力計画：第二フェーズ（1990～1995）最終報告書

日本原子力研究所東海研究所環境安全研究部
（編）馬場　恒孝・Kaye P. HART*

（1996年5月1日受理）

1980年代初めの技術的及び外交的な話し合いの結果、研究協力計画は最初5カ年計画（第一フェーズ）として1985年に始められた。この間、ＪＡＥＲＩとＡＮＳＴＯ間の人員派遣及び技術的なワークショップの開催を通じて、効率的な情報交換の成果をあげることができた。これらの成果を受け、当初の目標を達した第一フェーズに引き続き、更なる5カ年計画（第二フェーズ）が1990年に始められた。第二フェーズの計画では、（イ）ＰＷ－４ｂ模擬廃棄物を含むキュリウム添加シンロックの研究、（ロ）長寿命アクチニド元素のシンロック固化の研究、及び（ハ）処分条件下でのシンロック挙動の研究を目標とした。

研究協力の主な活動は、長期耐久性に関する研究で、再処理プロセスの特殊性に依存しない本来の高レベル廃棄物を模擬したＰＷ－４ｂ廃棄物を含むキュリウム添加シンロック、キュリウム添加単相ジルコノライト並びにキュリウム添加単相ペロブスカイトの作製とそれらのα加速試験及び各種特性試験、さらに地質年代にわたって安定に存在した天然ジルコノライトの特性を調べる試験であった。キュリウム添加試料の作製はＪＡＥＲＩの廃棄物安全試験施設（ＷＡＳＴＥＦ）で実施され、試験を遂行する際必要に応じＡＮＳＴＯから技術的な情報や助力が提供された。試験内容は、シンロックを処分した場合の10万年の期間に相当する試料が被るα崩壊損傷の影響を調べようとするものであった。結果は、本報告書で詳述するが、シンロックシステムの適用性評価において極めて重要なものであり、シンロックによる放射性核種の不動化性能を理解する上にも大いに役立つものである。これに加えて、ＪＡＥＲＩとＡＮＳＴＯは、キュリウム添加シンロックのα加速試験から派生した問題点を解決するため、関連する多くの研究を平行して行った。

第二フェーズの研究協力計画の全般的な成果は、双方の担当者間ですばらしい協力関係を継続したことと代替固化体としてのシンロックの潜在的な利点と限界について理解が深まったことであ

この報告書は、高レベル放射性廃棄物処理処分技術の研究開発における日本とオーストラリアの協力計画の第二フェーズの5年間（1990年から1995年）の成果をまとめたものである。

東海研究所：〒319－11　茨城県那珂郡東海村白方白根２－４
＊オーストラリア原子力科学技術機構：New Illawarra Road, Lucas Heights, NSW 2234, Australia

る。同時に、キュリウムの浸出性に及ぼすキュリウム添加量の影響を明らかにする研究、ジルコノライトが安定に存在する地質条件を確定するためのナチュラルアナログの研究及び種々の処分条件下におけるシンロックからの廃棄物成分溶出の長期予測モデルの開発の必要性が認識された。

当初の大半の目標を達成した第二フェーズ計画を1998年まで延長し、前述の課題に取り組み、研究協力の全体的なまとめを行うと共にシンロックシステムの適用性評価を行うよう強く要請する。

Contents

目　　次

1. INTRODUCTION

1.1 Historical Outline

The detailed history of the initiation of the Co-operative Program between ANSTO and JAERI is given in the Phase I report[1]. At the end of the Phase I Program, it was agreed that the Program should be extended into Phase II, a second five-year program to be carried out during 1990 and 1995.

1.2 Program Management and Formal Structure

The overall management of the Program was assigned to a Co-ordinating Committee which consisted of representatives of the respective government departments - the Science and Technology Agency (STA) from Japan and the Department of Resources and Energy (DRE) [later replaced by the Department of Primary Industries and Energy (DPIE)] from Australia - and the designated institutions — JAERI (in collaboration with the Power Reactor and Nuclear Fuel Corporation - PNC) and ANSTO [in full partnership with the Australian National University (ANU)]. The Co-ordinating Committee has met nine times at approximately 18 month intervals, with meetings alternating between Japan and Australia and with a Chairman provided by the Government Department in the host country. Details of these meetings held in Phase II are given in Appendix 2 of this report. (Details of other meetings are given in the Phase I report.)

In addition to the Co-ordinating Committee, the Implementing Arrangement provided for the establishment of a Steering Committee to review the technical progress of the Co-operative Program and to discuss future plans, including personnel exchanges. The Steering Committee meets at least once a year in either Japan or Australia with the chairman provided by the host institution, and receives reports on technical progress from the lead institutions. The Steering Committee reports to the Co-ordinating Committee. There have been a total of 20 meetings held; 10 in Phase II (see Appendix 2 for details of Phase II and the Phase I report for further information).

1.3 Program Objectives

The responsibilities of the two co-operating organisations for 1990-95 were laid down in the Phase II agreement. In broad terms the objectives of the program were to collaborate on Synroc research and development with an emphasis on each organisation complementing the other's work and on maximising exchange of information, results and personnel. The tasks carried out by the two lead organisations between 1990 and 1995 are given in Appendix 1 and below.

JAERI responsibilities

JAERI will continue alpha acceleration test for standard SYNROC and evaluate the performance and capability of SYNROC as a waste form for high-level radioactive wastes.

JAERI will prepare samples of SYNROC containing TRU elements on the basis of hot cell techniques accumulated in JAERI and upon information provided by ANSTO.

JAERI will conduct fundamental research on TRU immobilisation mechanism and study the matrix stability of SYNROC by long-term durability test under the collaboration between ANSTO and JAERI.

JAERI will collaborate in evaluating capability and feasibility of SYNROC system in the high-level waste and TRU waste management based on the results obtained through the cooperative studies described in this Appendix.

ANSTO responsibilities

ANSTO will continue to assess the radiation performance of SYNROC by studies which will include neutron irradiation and natural mineral analogues, and will cooperate with JAERI in the continued evaluation of alpha stability tests.

ANSTO, in collaboration with the Australian National University, will study the formulation, testing and optimisation of SYNROC for immobilisation of TRU elements from the perspectives of waste partitioning, FBR wastes, higher burnup LWR fuel, and other TRU streams.

ANSTO will conduct fundamental research on TRU immobilisation mechanisms, including matrix stability, by structural, leaching and geochemical modelling studies involving SYNROC containing simulated wastes and actinides.

ANSTO will collaborate in evaluating capability and feasibility of the SYNROC system in the high-level waste and TRU waste management based on the results obtained through the cooperative studies described in Appendix 1.

1.4 Personnel Exchange

There have been reciprocal visits of staff attending meetings of the Co-ordinating and Steering Committees and 11 longer-term exchanges of staff (see Appendix 3 for details).

1.5 Workshops

One workshop was held during Phase II of the Co-operative Program. This workshop allowed the dissemination of research results, encouraged technical information exchange and permitted detailed technical discussion of topics of current interest. Details of this workshop are given in Appendix 4.

2. REFERENCE SYNROC ACCOMMODATING SIMULATED PW-4b WASTE

2.1 Background

Studies have been made of the ability of Synroc containing simulated PW-4b waste to incorporate actinide elements. At ANSTO, samples containing low levels of Np, Am, Pu and Cm were fabricated in the mid-1980s to investigate the aqueous leaching behaviour of these elements. At JAERI, comparable samples of Synroc were made containing ~ 1wt% of ^{244}Cm to study accelerated α–decay damage analogous to that experienced by waste forms over extended timescales.

2.2 Fabrication of Cm-Doped, Reference Synroc

The nominal composition of the Cm-doped, simulated PW-4b waste is shown in Table 2.2.1.

Table 2.2.1 Composition of Cm-doped, simulated PW-4b HLW.

Element	Content (wt%)	Element	Content (wt%)
SrO	2.52	Cs_2O	8.42
Y_2O_3	1.44	BaO	3.82
ZrO_2	11.43	CeO_2	11.43
MoO_3	11.96	Nd_2O_3	6.90
RuO_2	7.26	CmO_2+PuO_2	21.50
Rh_2O_3	1.38	Fe_2O_3	3.70
PdO	3.48	Cr_2O_3	0.84
Ag_2O	0.19	NiO	0.34
CdO	0.29	P_2O_5	1.64
TeO_2	1.42		
Total			100.00

Initially, the hydroxide-route precursor for reference Synroc was mixed in a cold laboratory with simulated PW-4b waste, excluding the Cm source. The feedstock was then transferred to the hot-cell line. The Cm source of 1.639g was dissolved in the hot cell in teflon containers, in a mixture of 46.3g of concentrated nitric acid (density: 1.38 g cm^{-3}, HNO_3: 61%) and 0.1 mL of hydrofluoric acid (density: 1.15 g cm^{-3}, HF; 46.5%). During the dissolution, the temperature was maintained at 60°C. After decanting the solution, some undissolved material

remained at the bottom of the Teflon container; these deposits were collected. The weight of the undissolved material was 0.054 g (dry basis). Therefore, 1.585g of the Cm source was actually dissolved into the Cm stock solution. An aliquot, 0.1 mL, of the Cm stock solution was collected to measure ^{244}Cm activity. The remaining 99.6% of original Cm stock solution was incorporated into solid Synroc samples.

The Cm stock solution was poured into the slurry mixture of the precursor and simulated PW-4b waste, and mixed with a teflon-coated magnetic stirrer. After that, the pH of the mixture was adjusted to 9 using ammonium hydroxide. The mixture was dried and then calcined at 750°C for 2 hours under a stream of Ar + 4%H_2 gas. Recovery of the calcined powder was 97.8%. Minor losses of the calcined products occurred due to adhesion to the propeller, shaft and pot wall.

The pour and tap densities were measured. The calcined products were poured into a graduated polyethylene cylinder through a polyethylene funnel. Four independent readings of the level of the top surface were made to reduce errors. The average pour and tap densities of the two batches were 0.6 (± 0.05) and 1.12 (± 0.04) g cm^{-3}. Both batches of calcined products were mixed with 2 wt% titanium metal powder (<325 mesh) and then mixed using a twin-cone blender at 60 rpm for 15 mins; after this the mixture was divided into five equal parts to make block samples, designated herein as S9001 to S90005. Each part (13.21g) of the powder mixture was hot pressed in a graphite die in a flow of nitrogen gas.

The heating and pressing schedule was as follows:

(1) pre-pressing at room temperature and 29 MPa for 5 mins
(2) pressure was released
(3) the sample and the graphite die were heated from room temperature to 1150°C in 30 mins, to 1200°C in 10 more mins and kept at the same temperature for 10 more mins
(4) samples were hot pressed at 1200°C and 29 MPa for 2 h, and
(5) after hot pressing, the pressure was released, and the graphite die was cooled down to 300°C in 3 h and thence cooled to room temperature.

For sample S90001, the heating and pressing schedules were as above except that the graphite die was cooled down to 900°C in 1 h and then naturally cooled to room temperature. However for sample S90002, the thermocouple failed after 1-hour hot pressing so that power was lost and the sample cooled naturally from 1200°C to room temperature. (This sample was not used in further tests). The average weight of the as-cast block samples was 13.03 (± 0.01) g. The average weight loss was 1.4% during hot pressing, which was considered to be due to volatilisation and/or adhesion to the graphite die.

Peripheries of block samples were polished with #600 abrasive paper and their flat faces were finished with 6 μm diamond paste. After density measurement, (see Section 2.4) two of the polished block samples, S90003 and S90004, were sliced horizontally into five

discs and then each disc was cut across its diameter to obtain specimens for leach testing. All flat faces were finished with 6 μm diamond paste.

These specimens nominally contained 10.90, 87.12 and 1.98 wt% of simulated PW-4b waste, precursor material and titanium metal, respectively. The respective specific ^{244}Cm and total alpha activities of the samples were 27.4 (0.741) and 27.5 GBq g^{-1} (0.744 Ci g^{-1}) on February 28, 1990.

2.3 Phase Chemistry Studies of Actinide-Doped, Reference Synroc

Microscopy Studies. Blackford et al.[2] have recently carried out an AEM study on a suite of actinide doped Synroc specimens prepared by ANSTO. Their results showed that Pu and Np were preferentially incorporated in zirconolite by factors of 5 and 10, respectively, over perovskite on a wt% basis. No actinide partitioning into hollandite was observed. Furthermore the microstructures and phase distributions observed in these actinide-doped Synroc samples were similar to those seen in specimens containing simulated HLW fabricated in the open laboratory.

XRD. X-ray diffraction studies were undertaken at JAERI on the Cm-doped, Synroc samples prepared in their hot cell facilities. Figure 2.3.1 shows XRD patterns from a Cm-doped sample that had accumulated a dose of 12.4 x 10^{17} α decays.g^{-1} (equivalent age; 16,000 yr), before and after annealing at 800°C for 12 h in a graphite crucible. These X-ray patterns showed that the specimen consisted of the usual phases, hollandite, perovskite, and zirconolite. Unidentified minor peaks are possibly due to a hibonite phase. Peak intensities of zirconolite and perovskite, relative to that of the (130)/(310) hollandite peak are less in the as-damaged condition than in the annealed state. This result reflects the fact that the short-range, actinide recoil nuclei cause atomic disorder in their host phases and that hollandite is less affected by α-decay damage.

2.4 Physical Properties of Cm-Doped, Reference Synroc

The densities of 2-cm-diameter x 1-cm-high cylinders (S90002 and S90005) were periodically measured by the water displacement method. Two samples were cut from another cylinder (S90001) and annealed at 1000°C for 2 h in a graphite crucible. After heat treatment, one sample (R1-5) was stored at 200°C, and the other (R1-6) was stored at room temperature. Densities of these samples were measured periodically in the same manner as above. The effect of α-decay damage on density for samples S90002 and S90005 is shown in Figure 2.4.1. The rate of density change with increasing α-decay dose was essentially constant, suggesting that thus far no macrocracking due to volume swelling had occurred. Figure 2.4.2 shows that storage of the sample at 200°C reduced the change in density per unit α-dose by a factor of 2 compared to that of the sample stored at room temperature.

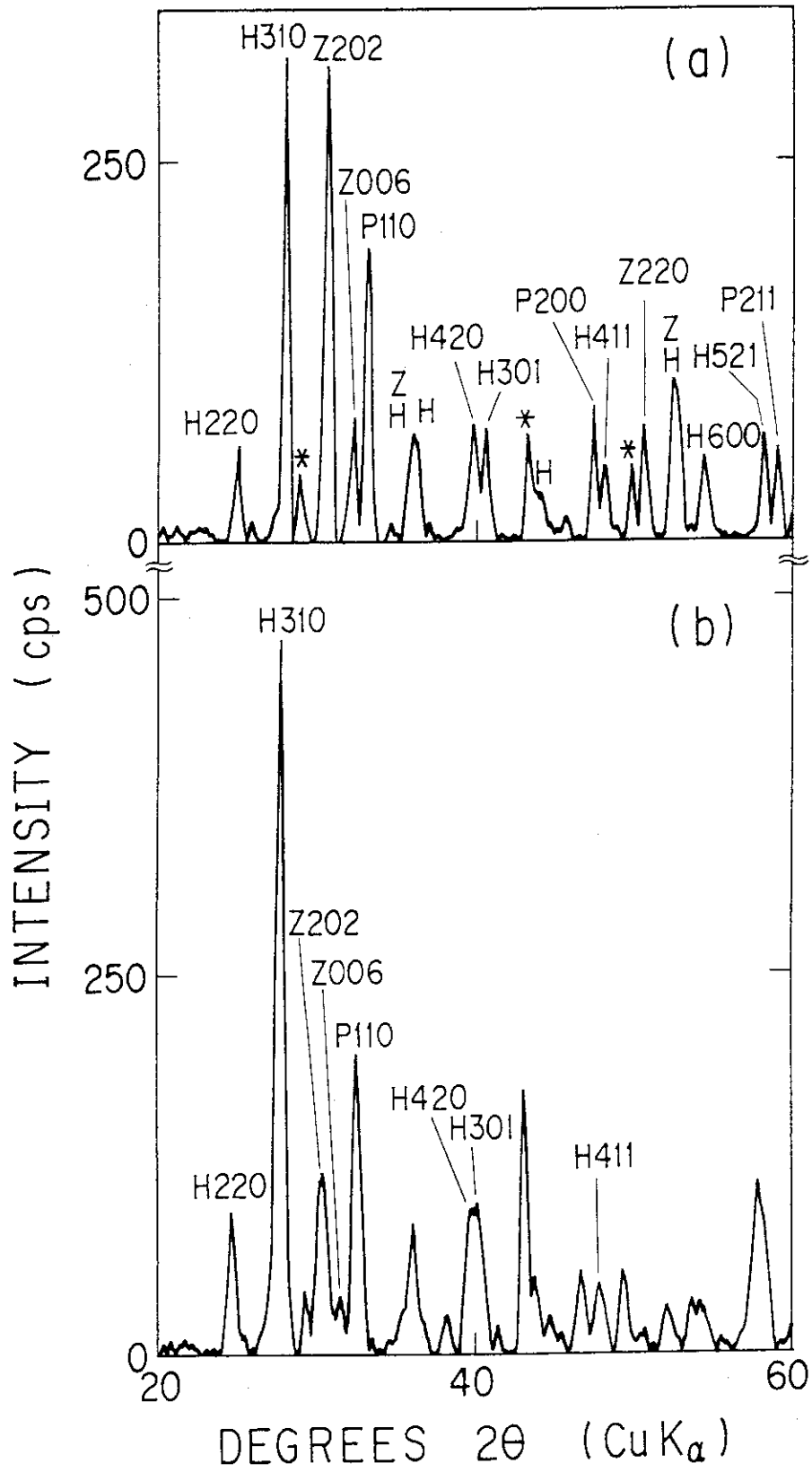

Figure 2.3.1 X-ray diffraction patterns from (a) annealed and (b) as-damaged Cm-doped, reference Synroc containing simulated PW-4b waste. The sample was subjected to a dose of 12.4 x 10^{17} α decays g^{-1}, and then annealed at 800°C for 12 h.

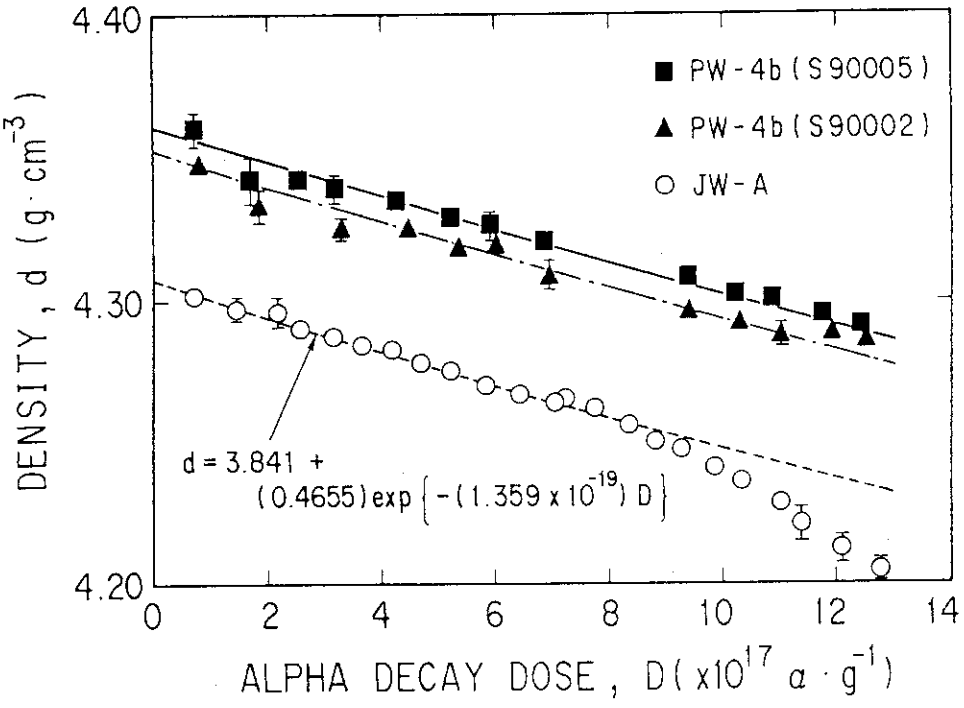

Figure 2.4.1 Densities of two kinds of Cm-doped Synroc versus α–decay dose. Samples S90002 and S90005 were hot-pressed at 1200°C/29 MPa for 1 h and 2 h.

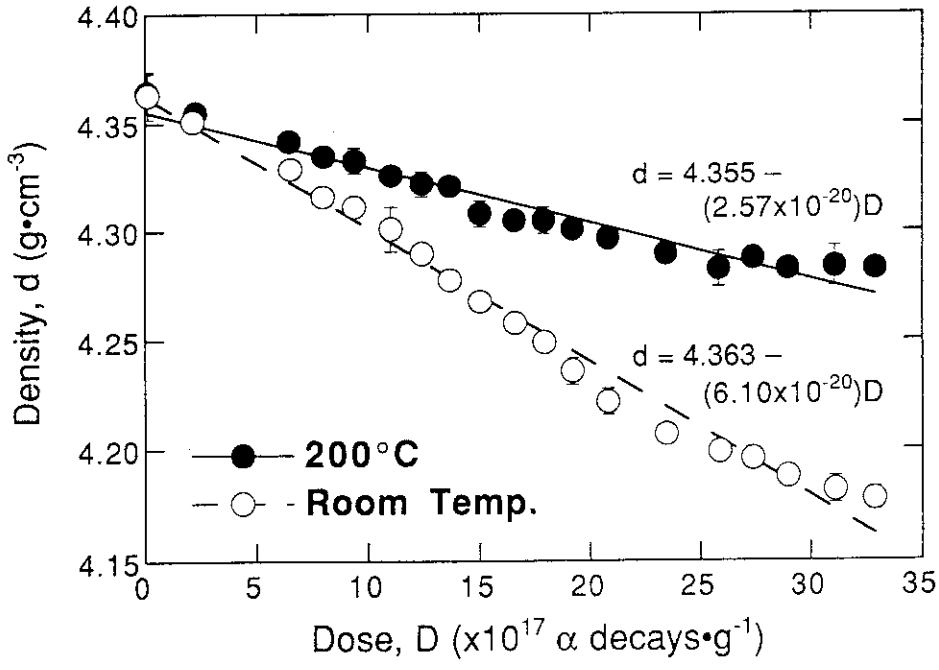

Figure 2.4.2 Effect of storage temperature on the relationship between density and α–dose.

2.5 Leaching Behaviour of Actinides Released from Reference Synroc

2.5.1 Studies at ANSTO of actinide-doped Synroc

Figure 2.5.1 compares the normalised solution leach rates of Np, Pu, Am and Cm in deionised water at 70°C. The leachability of the actinide elements decreased in the order: Np > Am > Pu > Cm. Typically, most of the Np is in solution (83%), in contrast to the other actinides where most of the activity released into solution was associated with the vessel walls. Moreover, the leach rates of the actinides decreased with time and the overall results confirmed that, as a group, these elements are the least leachable of all the HLW elements.

The releases are not dominated solely by the solubility of each element in the aqueous solution; rather there is a relationship between the overall release of the actinide elements into solution and the matrix leach rate. Figures 2.5.2 to 2.5.5 show the concentration of actinides in solution and associated with the vessel wall as a function of leaching duration. It is apparent that increasing the leaching time does not generally increase the concentration of the actinides in solution or, more importantly, on the vessel wall, so longer leach periods appear to be associated with decreased matrix dissolution rates of Synroc.

The leaching results, which suggest that Np release is not being controlled by the formation of secondary, surface phases, are consistent with the microscopy results[3] that showed that none of the secondary, surface phases contained Np.

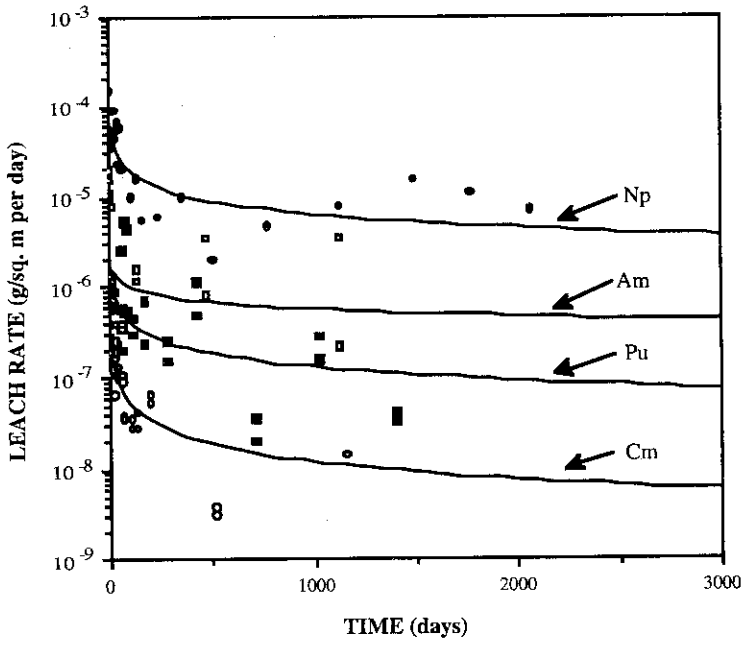

Figure 2.5.1 Solution leach rates of Np, Pu, Am and Cm in deionised water at 70 °C.

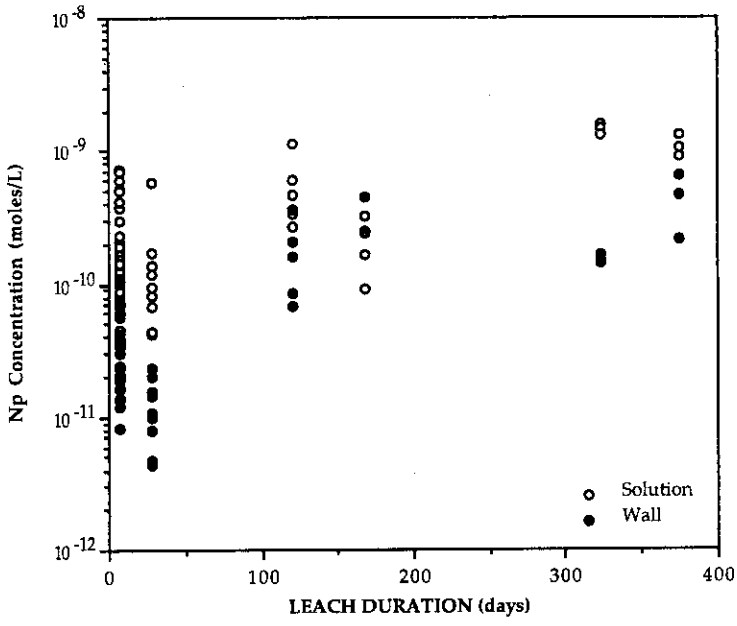

Figure 2.5.2 Effect of leach duration on Np concentration in solution (at 70°C in deionised water) and associated with the vessel walls.

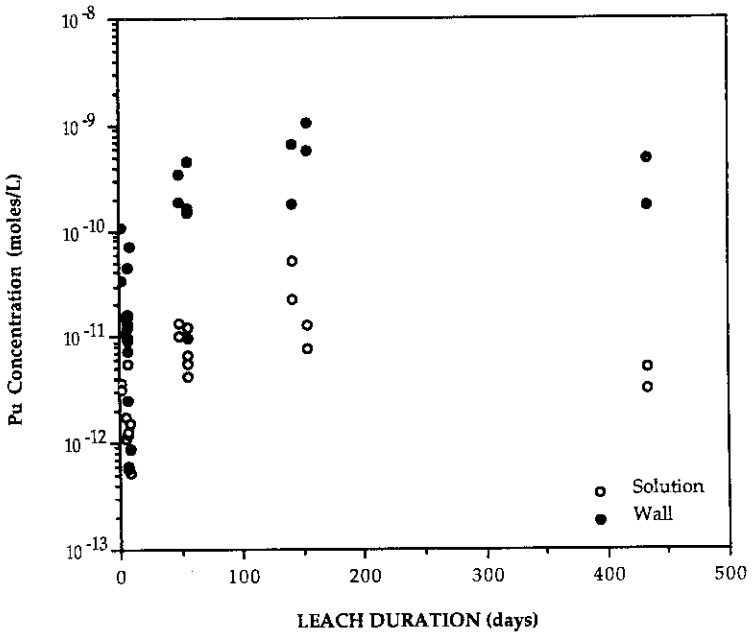

Figure 2.5.3 Effect of leach duration on Pu concentration in solution (at 70°C in deionised water) and associated with the vessel walls.

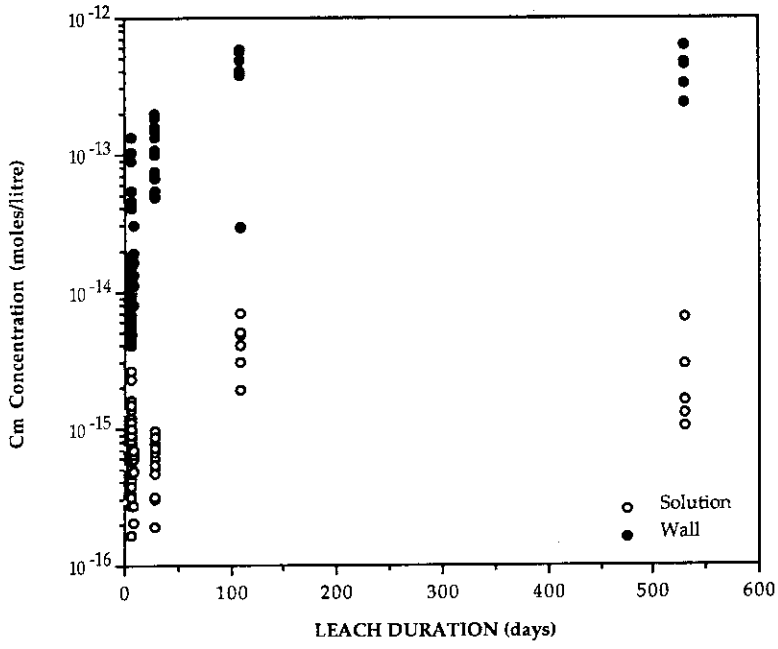

Figure 2.5.4 Effect of leach duration on Cm concentration in solution (at 70°C in deionised water) and associated with the vessel walls.

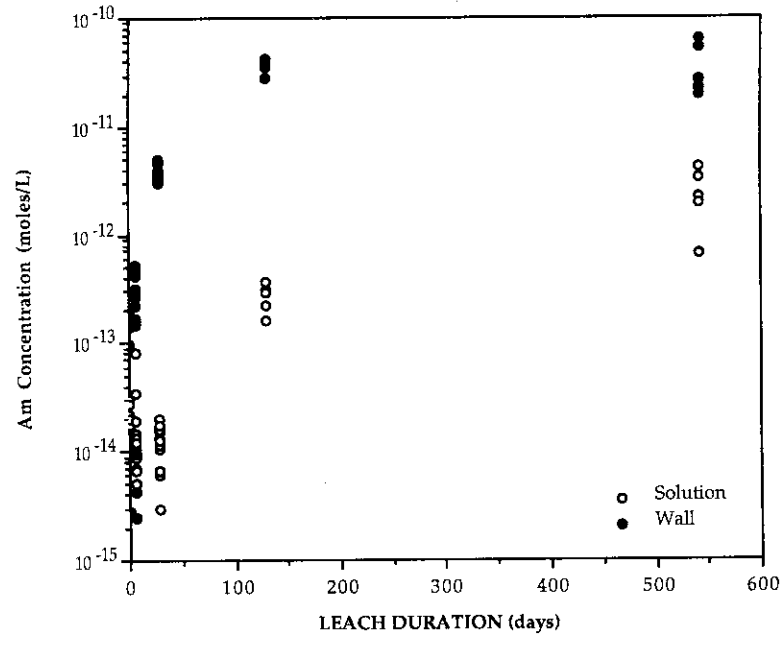

Figure 2.5.5 Effect of leach duration on Am concentration in solution (at 70°C in deionised water) and associated with the vessel walls.

2.5.1.1 Leaching under anoxic conditions

Studies under anoxic conditions have been carried out in a glove box with a nitrogen atmosphere containing less than 20 ppm O_2. All filtration procedures were completed within the glove box and the filtrates were acidified before they were removed.

Np-doped Synroc. Leaching of Np-doped Synroc samples in deionised water at 70°C has been carried out in the open laboratory and under an anoxic atmosphere. This study[4] was carried out as an initial measure of the effect of anoxic conditions on the release of Np and was further supplemented with work carried out on releases under anoxic conditions in the presence of geological materials (see below). The studies in deionised water showed that;

- Solution leach rates under oxic conditions were similar to those measured under anoxic conditions. However, under oxic conditions most of the leached Np (83%) was in ionic form, while under anoxic conditions, filtering of the solution through a 0.45 μm filter reduced the activity of Np by a factor of 24, suggesting that the leached Np was predominantly associated with fine particulates.
- From available data, the measured concentrations of Np in solution in this study are lower than the predicted solubility limits, suggesting that the solubility of Np is not controlling the release from Synroc under either oxic or anoxic conditions. This is consistent with the results obtained for different leach durations detailed above.

Interaction with geological materials. Leaching of Np-doped Synroc in the presence of Mol clay under an anoxic atmosphere[4] has established that;

- Under anoxic conditions the differential leach rate of Np is low (5×10^{-5} g m^{-2} d^{-1}) and not enhanced by the presence of Boom clay.
- In deionised water the soluble Np fraction measured under anoxic conditions is a factor of 10 lower than under oxic conditions, but the total release of Np from the sample under both conditions is similar.
- Within experimental error, the presence of Boom clay did not markedly affect the distribution of Np between the solution and filterable colloidal components of the solution.

The smaller soluble Np fraction measured in deionised water under anoxic conditions, compared to clay-buffered leachates, probably results from the formation of very insoluble species, such as oxides, of the radionuclides in the poorly buffered deionised water. The above results reinforce that leach rates and radionuclide solubilities must be measured under geologically relevant conditions if the results are to be used for performance assessment purposes.

2.5.2 Studies at JAERI of Cm-Doped Synroc

Half-disc specimens of Cm-doped Synroc have been leach tested in triplicate using the MCC-1 test method at 90°C for 56 days, with four, seven-day leach periods followed by a 28 day period. After pH measurement and addition of 0.1 cm^3 concentrated nitric acid, leachate samples were withdrawn from the glove box and subjected to NaI (Tl) γ-ray spectrometry and liquid analyses using ICP/AES (Ca, Mo and Ba) and AAS (Cs and Sr) in the same way as in the Phase I co-operative work.

Cm-doped Synroc samples containing simulated PW-4b waste which had accumulated different levels of α-decay damage corresponding to equivalent ages of (a) 50, (b) 430, (c) 13,000 and (d) 30,000 years were leach tested as above. Figures 2.5.6 and 2.5.7 show the change in average leachate pH and Eh as a function of leaching time. Generally, the pH of specimen-charged leachates is lower than that of the blank leachate, except for the most damaged specimen where the two pHs are very similar. For all leach tests, the average Eh of the specimen-charged leachate is similar to that of the blank leachate, with the exception of the final leaching period where for the more damaged specimens the Eh of the specimen-charged leachate is lower.

Figure 2.5.8 summarises the leach rates of inactive elements with time. The leach rates of equivalent cold samples are compared to those of Cm-doped, simulated PW-4b containing samples that had accumulated different levels of α-damage. The leach rates of Mo, Ca, Sr, Cs, and Ba measured for the sample that had accumulated damage equivalent to 50 years of storage were similar to those for the cold sample, varying by less than one order of magnitude.

In all cases, the leach rates decrease quickly with time. However, with increasing damage the rate of decrease is smaller. The leach rates of inactive elements decrease in the following order:

$$Mo > Ca \approx Sr > Ba$$

The leaching behaviour of Cs is complicated. For specimens with equivalent ages of 50 and 430 years, the leach rates of Cs and Ba are similar but for more damaged specimens the Cs leach rate is a factor of between 5 and 10 higher than that of the 50 year sample (see Figure 2.5.8). The increase in Ca and Sr leach rates is less marked and Mo and Ba leach rates do not vary significantly with increasing α-damage. The increase in Ca and Sr leach rates occurs with increasing α-decay damage to the perovskite phase. However, Cs and Ba are both incorporated in the hollandite phase, which does not incorporate actinide elements, but at this stage, it is not possible to explain the enhanced release of Cs over Ba from the more damaged specimens.

Figure 2.5.9 shows the effect of time on the average total leach rates of ^{244}Cm for the specimens with equivalent ages of 50, 430, 13,000, 30,000 and 113,000 years. The leach rates do not change significantly with increasing α-damage, and are instead apparently controlled more strongly by the pH of the leachant.

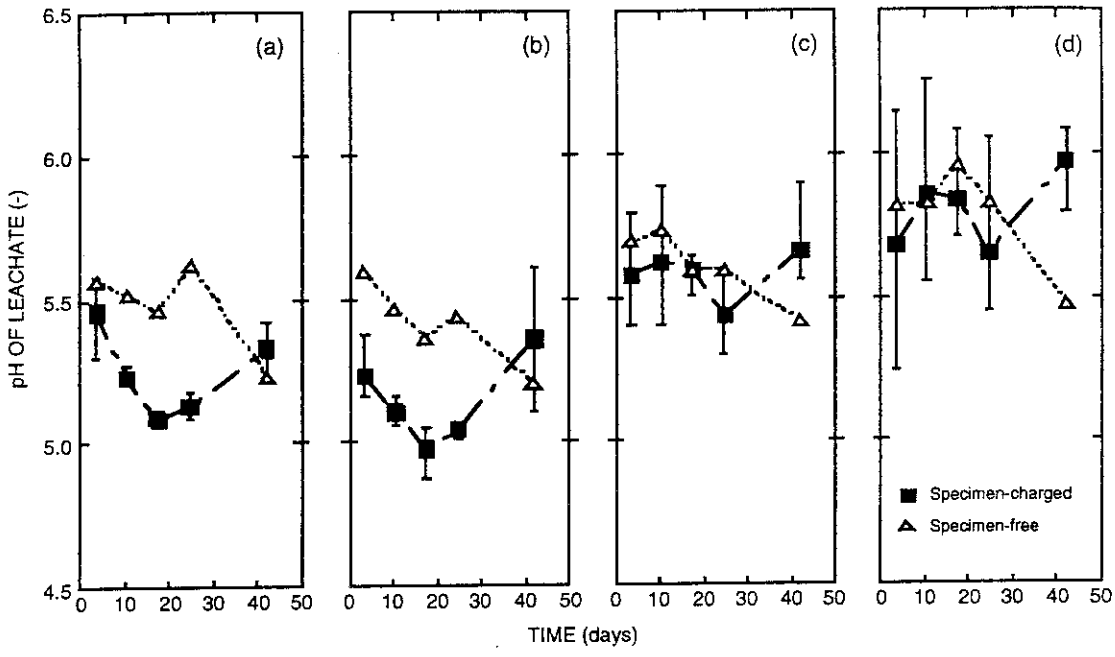

Figure 2.5.6 Change in pH of leachate from Cm-doped, reference Synroc vs leach time.

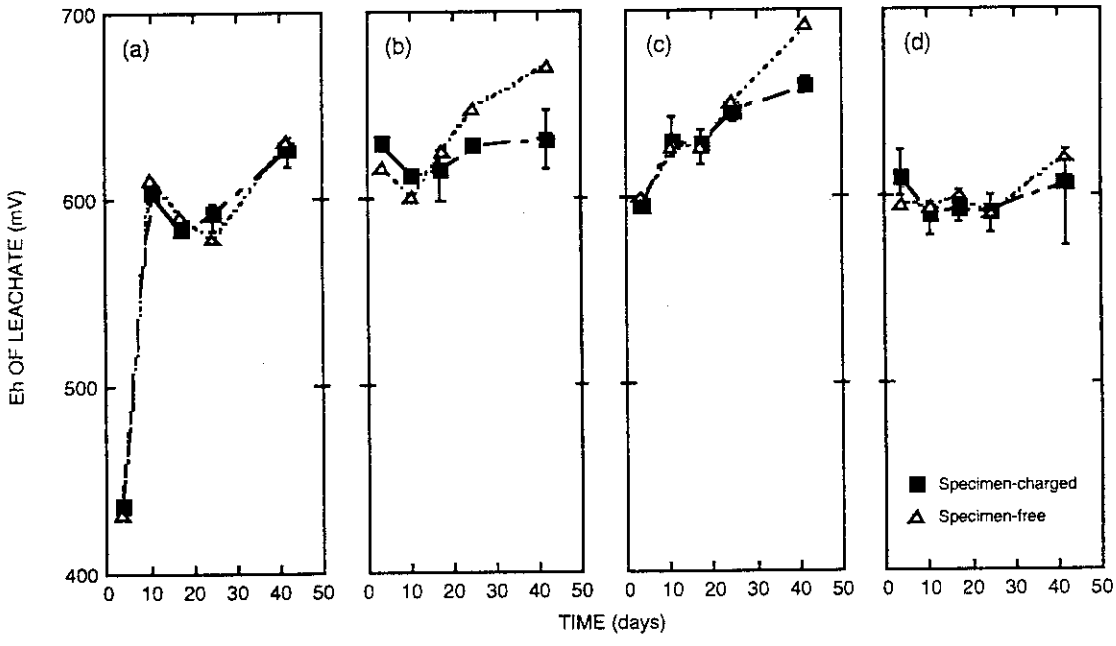

Figure 2.5.7 Change in Eh of leachate from Cm-doped, reference Synroc vs leach time.

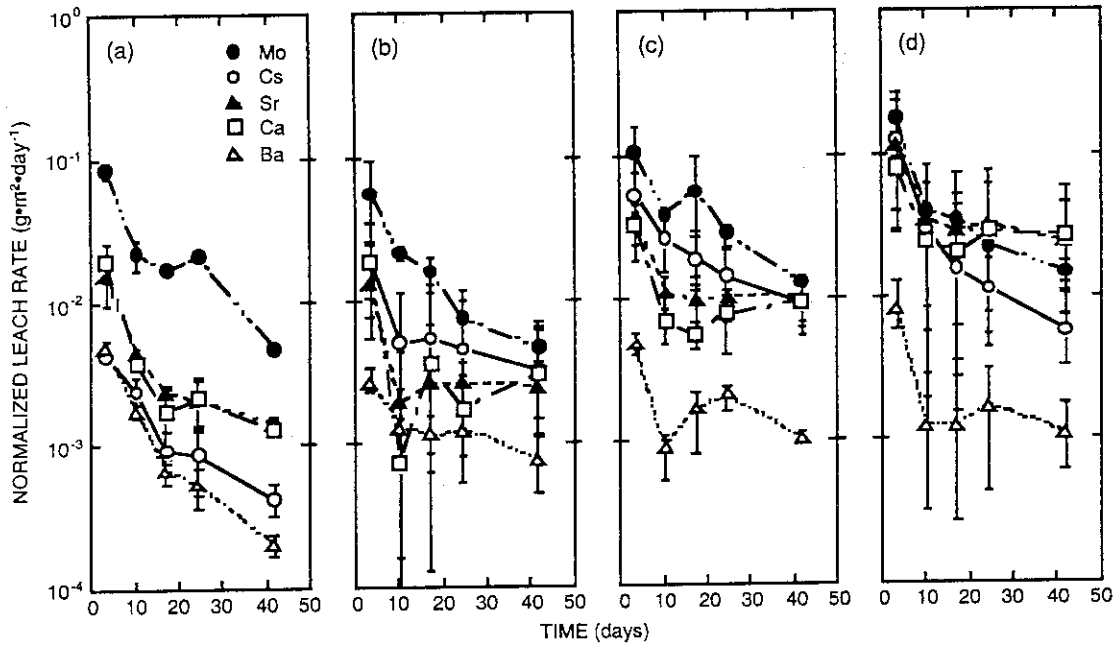

Figure 2.5.8 Comparison of normalised leach rates of indicator elements from reference Synroc containing (a) non-radioactive PW-4b waste, and Cm-doped PW-4b waste, of different equivalent storage ages — (b) 50 years; (c) 430 years; (c) 13,000 years.

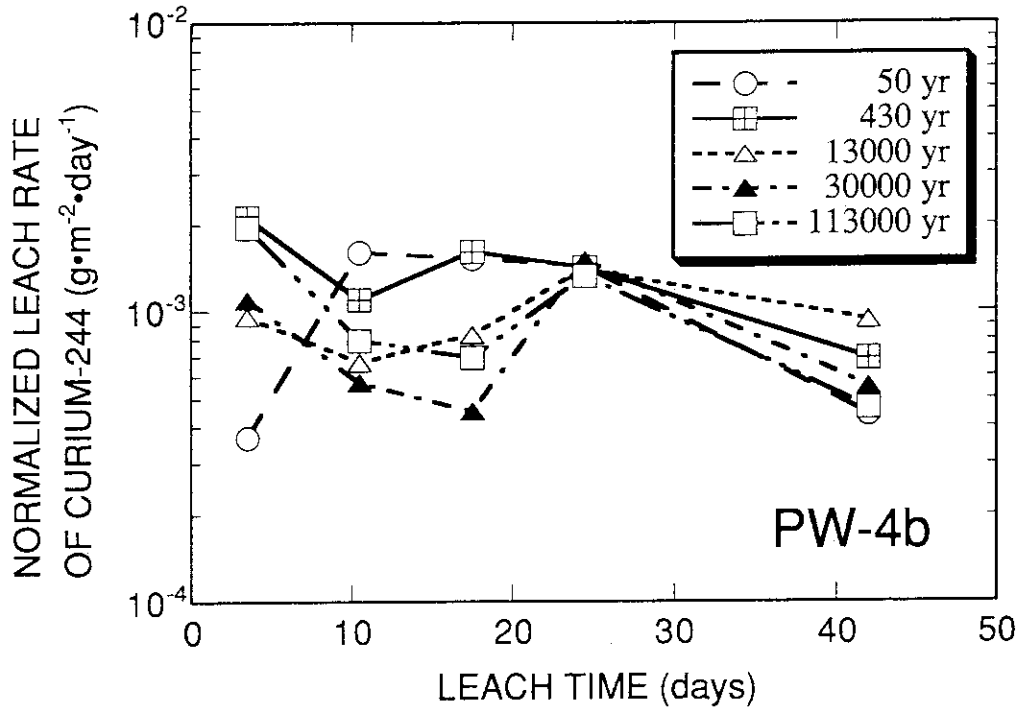

Figure 2.5.9 Comparison of normalised leach rates of ^{244}Cm from reference Synroc containing simulated PW-4b waste of different equivalent storage ages.

2.6 Comparison of Leach Tests Results Obtained for Reference Synroc in JAERI and ANSTO

The leach tests carried out on Cm-doped reference Synroc at JAERI and ANSTO have been discussed above. These results have shown that the leach rates of inactive elements from Synroc containing 0, 0.0004 and 0.91 wt% ^{244}Cm were similar. Confirming that the fabrication procedures used in the open laboratory, glove-box line and hot-cell facility and in the two organisations are comparable and reproducible.

Total Cm leach rates (i.e. unfiltered solution plus vessel wall) have also been measured at both organisations. Figure 2.6.1 shows all of the total Cm leach rate data collected at ANSTO. These data are similar to those collected at JAERI in that they show that the release of Cm tends to be constant and does not markedly reduce with time. However, the leach rates obtained at ANSTO are at least two orders of magnitude lower than those measured at JAERI. At this stage it is not possible to establish whether this is as a result of radiolysis of the leachates in the higher activity samples or if it has been caused by other factors. There is some evidence for radiolysis, in that Figure 2.5.6 shows that the pH in the specimen charged leachates is lower than the blank but further investigations are required to fully elucidate this effect. In the extension to the Phase II program a suite of samples containing a range of ^{244}Cm concentrations will be studied to determine the effect of the level of Cm-doping on leach rate.

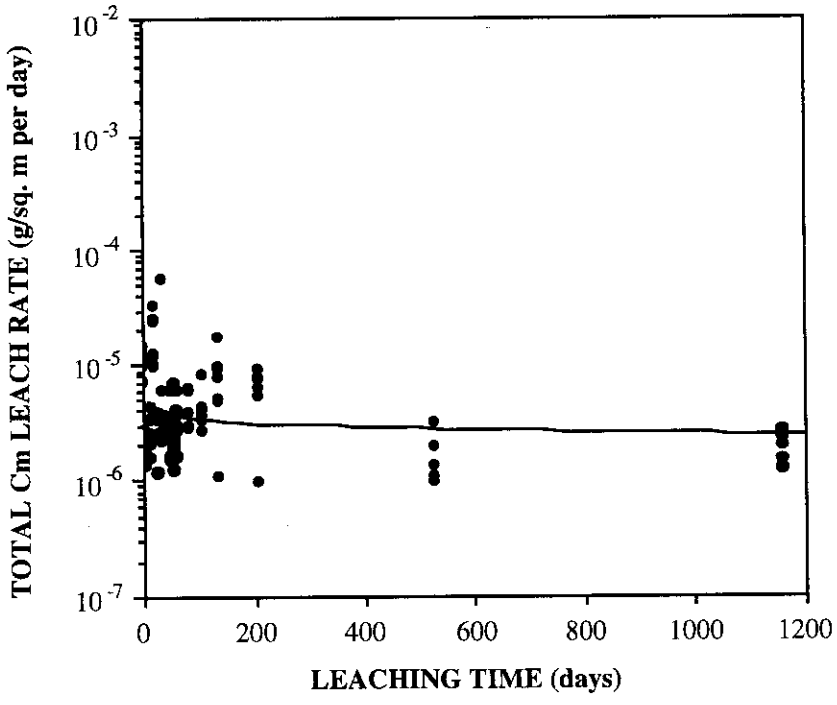

Figure 2.6.1 Total Cm leach rates measured at ANSTO in deionised water at 70°C for reference Synroc doped with 0.0004 wt% Cm.

3. STUDIES ON SINGLE PHASE PEROVSKITE SAMPLES

3.1 Background

In Synroc, actinide nuclides are incorporated in perovskite and zirconolite phases. As outlined in Section 2 of this report, α–decay damage effects were studied by doping Synroc with ^{244}Cm. However it is also informative to study α-decay damage effects in the host phases individually. In this Section, data obtained for 'cold' and Cm-doped perovskite, fabricated by JAERI from formulations supplied by ANSTO, are presented.

3.2 Fabrication of Cm-Doped Perovskite

On 31 March 1993, the Cm source included 39 mole% of ^{244}Cm, and 56 mole% of ^{240}Pu, a daughter nuclide of ^{244}Cm. If the actinides in the Cm source are assumed to be trivalent and incorporated in the calcium site of perovskite via an Al^{3+} substitution on a Ti^{4+} site see below, the following material should result;

$$Ca_{0.98919}An_{0.01081}Al_{0.01081}Ti_{0.98919}O_3$$

However, this is an approximation as some Ti^{3+} could be present, because of the reducing conditions imposed by the use of the graphite die for the hot-pressing step, displacing a small amount of excess Al^{3+}.

Figure 3.2.1 shows the preparation process. Cm (0.8165g) was dissolved in 40 g of concentrated nitric acid with 0.1 cm^3 of hydrofluoric acid, and then 20 cm^3 of 0.1 N nitric acid was added. From this stock solution 0.1 cm^3 was collected for α–analysis. After correction for this quantity, the Cm source (0.8140 g) was mixed with the precursor material (a slurry of $Ca(OH)_2$ mixed with TiPT and ASB).

The pH of the slurry mixture was adjusted to 9 with ammonium hydroxide. It was then poured into an in-cell calciner pot and dried at 80°C in a stream of N_2 gas, and then calcined at 750°C for 2 hours in a stream of Ar-4%H_2 gas; 36.7089 g of calcined powder was collected (97% recovery) and 22.2574 g was poured into a graduated polyethylene cylinder to measure its pour density.

The calcined powder was divided into three portions of 12.2616, 12.2462, and 12.2432 g. Each portion was hot-pressed using a graphite die at 1250°C and 29 MPa for 2 hours in a stream of N_2 gas. The three as-cast samples weighed 12.1002, 12.0930, and 12.0760g, respectively; corresponding to a weight loss of 1.3-1.4% during hot-pressing.

Specific ^{244}Cm and alpha activity of the samples, calculated from the mass assay, were 22.40 $GBq.g^{-1}$ (0.6053 $Ci.g^{-1}$) and 22.29 $GBq.g^{-1}$ on 31 March, 1993.

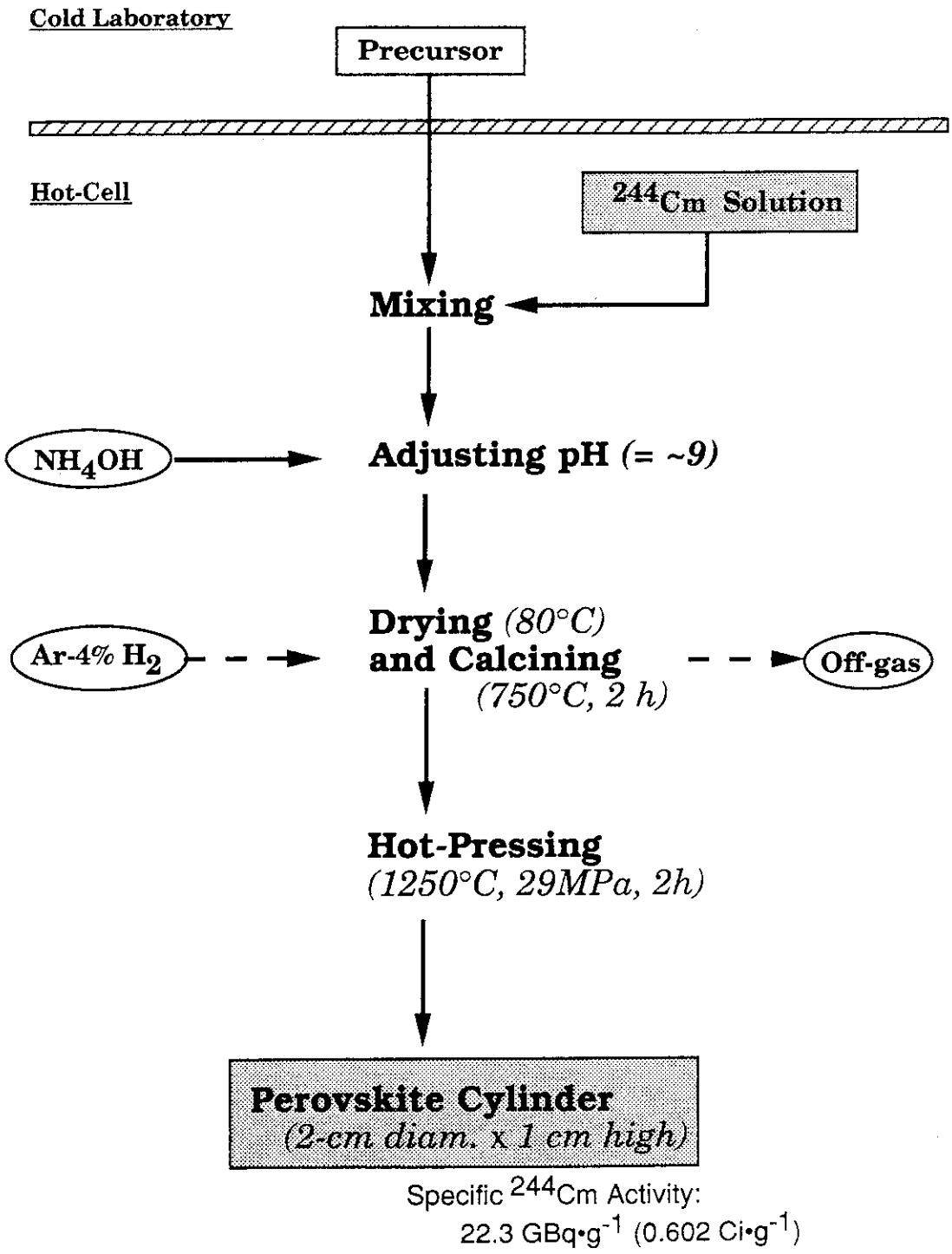

Figure 3.2.1 Preparation of Cm-doped perovskite.

3.3 Physical Properties of Cm-Doped Perovskite

Density. Pour and tap densities of the calcined products were 0.53 and 1.09 g cm^{-3}. The average density of the three hot-pressed samples was 4.083 $g.cm^{-3}$, one month after hot pressing when the samples had accumulated a dose of 7 x 10^{16} α $decays.g^{-1}$. The change in density of the Cm-doped perovskite cylinder is shown in Figure 3.3.1. The density changes are well fitted by a linear equation. At a dose of 9 x 10^{17} α $decays.g^{-1}$, the fractional density decrease of the Cm-doped perovskite was 1.3%. This value was in fair agreement with those of Vernaz et al[5] for ^{238}Pu-doped perovskite.

XRD. As-leached and annealed half-disk specimens were subjected to XRD. Surfaces of annealed specimens were finished with 6 μm diamond paste after the 800°C annealing in a graphite crucible. XRD data were collected at intervals of 0.05° over the 2θ range of 10-120°, using Cu K_α radiation.

Figure 3.3.2 shows X-ray diffraction patterns from annealed and as-leached specimens which had accumulated a dose of 5.6 x 10^{17} α $decays.g^{-1}$. The annealed specimen contained predominantly the perovskite phase although it also contained minor amounts of a phase (indicated by "*" on the pattern), probably $(Cm,Pu)O_2$. After leaching anatase (TiO_2) lines appear along with those of the above phases, in addition to the major phase which suggests formation of a surface film. The precipitation of anatase is consistent with leach data, which showed little solubilisation of Ti (see Section 3.4), compared to that of Ca and Cm.

3.4 Leaching Behaviour of Cm-Doped Perovskite

For leach testing, half-disk specimens of 2 cm in diameter and ~1mm in thickness were cut from the hot-pressed cylinders, P93001 and P93002, and their flat faces were polished with 6 μm diamond paste as in the previous work. The half-disk specimens were MCC-1 leach tested in a pH ~2 solution (0.05M KCl + 0.013M HCl) at 90°C for two months over four 7-day leach periods and a 28-day leach period. (This leachate was used for testing as it was postulated that the Cm leached from the Synroc would be soluble at this pH, but not under neutral conditions, and gross counting techniques could be used to assess the total leach rate without having to measure solution and vessel wall contributions to activity.) The leachate samples were analysed by γ-ray spectrometry for ^{244}Cm and ICP/AES for non-radioactive elements.

The weight losses of half-disk specimens after two-month leach testing were equivalent to average leach rates of 1.7, 2.3, and 3.0 $g.m^{-2}.d^{-1}$ from the Cm-doped perovskite material that accumulated doses of 1.6 x 10^{17}, 4.0 x 10^{17}, and 8.3 x 10^{17} α $decays.g^{-1}$, respectively (Table 3.4.1).

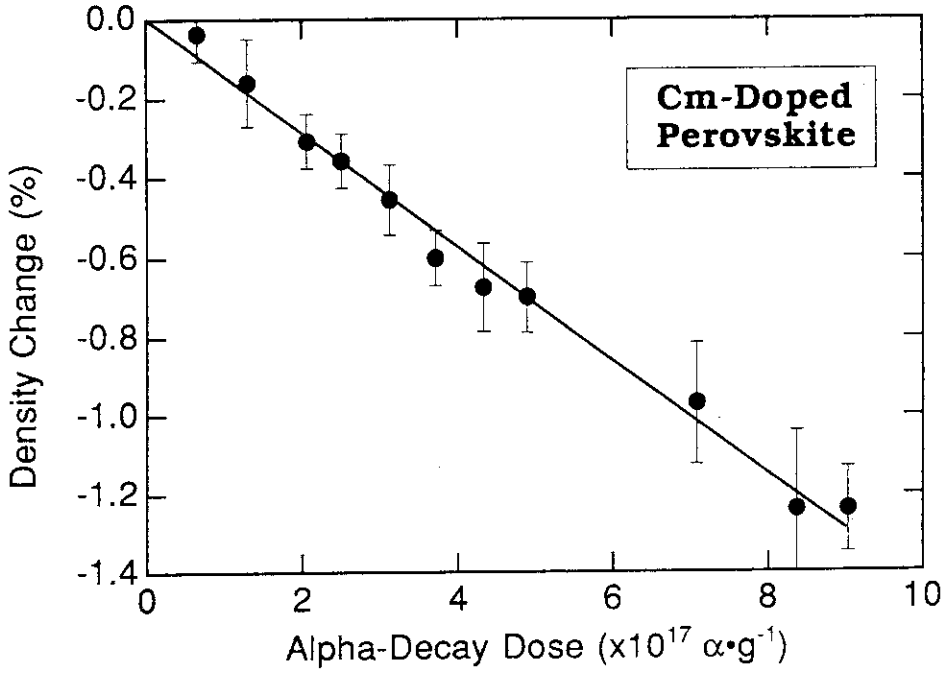

Figure 3.3.1 Change in density with increasing α–decay damage for Cm-doped perovskite.

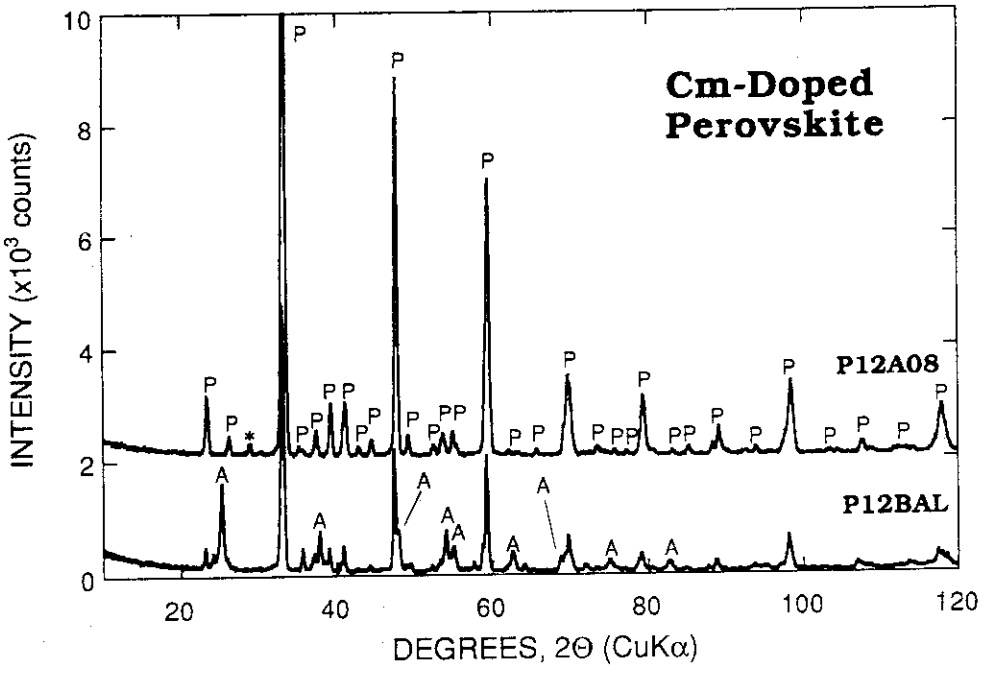

Figure 3.3.2 XRD Patterns from annealed (P12A08) and as-leached (P12BAL) Cm-doped perovskite specimens. (Cu Kα radiation.)

Table 3.4.1 Leach rates of Cm-doped perovskite (based on CaO loss).

Specimen Name	Leach Rate* A ($g\,m^{-2}d^{-1}$)	Leach Rate# B ($g\,m^{-2}d^{-1}$)	(A/B)x100 (%)	Dose (α- decays g^{-1})
P1-3B	0.93	1.28	73	1.6×10^{17}
P2-2B	1.47	1.77	83	1.6×10^{17}
P2-5B	1.97	2.08	95	1.6×10^{17}
Average	1.46	1.71		
P1-2B	1.88	2.07	91	4.0×10^{17}
P1-4B	2.22	2.43	91	4.0×10^{17}
P2-3B	2.43	2.46	99	4.0×10^{17}
Average	2.18	2.32		
P1-3A	2.98	3.04	98	8.3×10^{17}
P2-2A	2.94	3.02	97	8.3×10^{17}
P2-4A	2.85	2.78	103	8.3×10^{17}
Average	2.92	2.95		

*A: Derived from CaO weight loss
#B: Derived from total weight loss

Figure 3.4.1 compares changes in the normalised Ca leach rate and pH with leaching time. In this Figure, (1), (2), and (3) indicate leaching runs after doses of 1.6×10^{17}, 4.0×10^{17}, and 8.3×10^{17} α decays.g^{-1}, respectively. Unlike the normal leaching behaviour of Synroc, in which all leach rates decrease with increasing leaching time, the Ca leach rate from the Cm-doped perovskite initially increases with leach time. However it begins to fall again after ~ 25 days. The more damaged specimens tend to give a higher Ca leach rate. In the 28-56 day leaching period, the acidic leachant solution was partly neutralised by Ca^{2+}-proton exchange and the Ca leach rate for the samples which had accumulated three different doses converged to a similar value. Titanium concentrations in the leachates were near the limit of detection.

The γ-ray spectrometry also showed high leach rates of ^{244}Cm (Figure 3.4.2). The Ca and Cm leach rates were similar. In the final leaching period, the Cm leach rate was lower than the Ca leach rate by a factor of >20, no doubt due to the lower Cm solubility at the higher pH.

The leach rates given above for perovskite are higher than those measured for inactive samples at ANSTO. This discrepancy will be investigated further in the extension to the Phase II program using sample and technology exchange between both organisations.

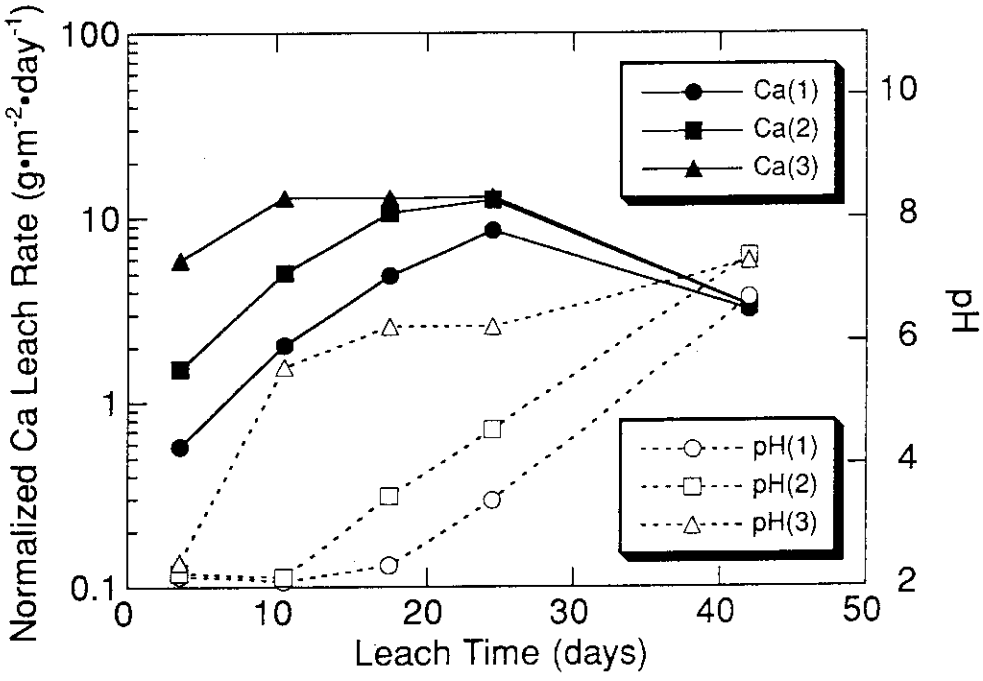

Figure 3.4.1 Comparison of the normalised Ca leach rate and pH with time.

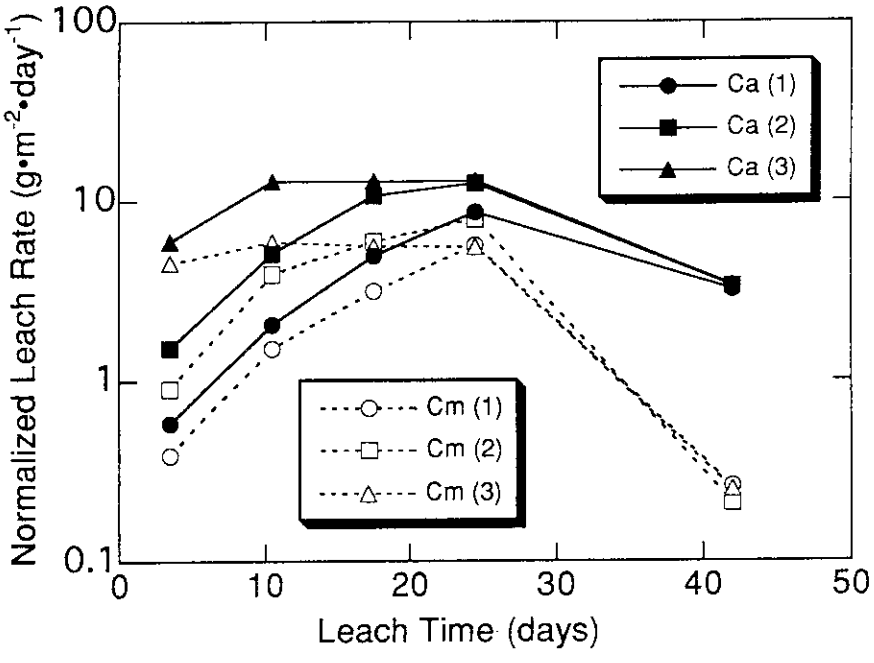

Figure 3.4.2 The normalised leach rate of Cm and Ca from perovskite.

4. MODIFICATION OF REFERENCE SYNROC TO ACCOMMODATE HIGH LOADINGS OF TRU WASTE

4.1 Background

Zirconolite is the primary host for actinides and comprises ~ 20 wt% of reference Synroc-C. It is the most durable phase in the reference Synroc formulation and has a high solid solubility for actinides. Accordingly, the development of a zirconolite-rich Synroc was a prime focus of the Phase II project.

4.2 Phase Chemistry Studies of Zirconolite-Rich Synroc

4.2.1 Non-radioactive specimens

We summarise below the crystal chemistry of zirconolite. Earlier studies on the incorporation of Nd, U, Np, into synthetic zirconolites were not always specific about valence states or substitution mechanisms[6 - 14].

In the present work we attempted to establish the valence state of selected substitutions of multivalent ions in zirconolite by a well-known strategy of synthesis. The basic idea is that nominal solid solutions tend to form a single-phase if at all possible, so that if a projected substitution of a guest ion of given valence in a given host site can be properly charge compensated, the appearance of the solid phase confirms the guest ion state.

Aqueous nitrate solutions of Ca, rare earths or actinides and any charge compensating ions such as Al, that were deemed necessary were mixed together. After stir-drying, the mixtures were calcined in air (for rare earths) or 3.5%H_2/N_2 (for actinides) at ~700°C to remove water, NO_x and organics. Final consolidation and equilibration of the rare earth samples was achieved by pelletising and sintering for 1-3 days at 1350-1400°C, with some intermediate grinding and re-sintering steps. While these temperatures are higher than those envisaged in Synroc production, the objective was to achieve equilibration by prolonged heating within ~100°C of the melting points (1525°C for pure $CaZrTi_2O_7$[15]). Consolidation of the actinide-bearing samples was achieved by hot-pressing in graphite dies of 1 cm bore at 1250°C/18 MPa for 2h to yield two 2 mm thick samples per pressing. A disadvantage of hot-pressing in graphite is that the reducing conditions promote the formation of a minor fraction of perovskite. The hot-pressed samples were reheated in air or neutral conditions to enhance equilibration.

XRD was carried out with conventional diffractometers on powdered rare-earth-containing samples, U-bearing samples were in the form of 1 cm diameter hot-pressed or sintered pellets, and the Np- and Pu-bearing samples consisted of hot-pressed pellets cut in half along their diameters, set in a resin, and finally polished to a finish of 1 μm. JEOL

scanning and transmission electron microscopes were used to characterise polished pellets and ion-thinned materials as appropriate.

Neodymium. Samples of nominal compositions $Ca_{(1-x-y/2)}Nd_{(x+y)}Zr_{(1-y/2)}Al_{(x)}Ti_{(2-x)}O_7$ were prepared. The successful synthesis of a single-phase zirconolite would imply that (x+y/2) atoms of Nd inhabit the Ca site and y/2 units the Zr site. Samples with y = 0 and x up to 0.65 were found to be single phase, monoclinic zirconolites. However, for x = y = 0.1-0.3, samples all showed perovskite in addition to zirconolite. For x = 0.7-0.85 an orthorhombic phase was observed and at x > 0.85, additional phases such as zirconia and alumina were observed. TEM studies of x = 0.5 (y = 0) material showed the zirconolite crystallites were of the 2M polytype with very few lattice defects. It was concluded that the respective solid solubilities of Nd^{3+} in the Ca and Zr sites were ≈ 0.7 and 0.2 formula units, and that the Nd^{4+} ion was not stable in zirconolite.

Cerium. The crystal chemistry of cerium in zirconolite was characterised using three samples. In sample Ce-1 of nominal composition $Ca_{0.8}Ce_{0.2}ZrTi_{1.8}Al_{0.2}O_7$, the formation of a single phase would imply that Ce was in the +3 state and substituted on the Ca site, with Al^{3+} as a charge compensator on a Ti site. Samples Ce-2 and Ce-3 of nominal compositions $Ca_{0.8}Ce_{0.2}ZrTi_{1.6}Al_{0.4}O_7$ and $CaZr_{0.8}Ce_{0.2}Ti_2O_7$ would have Ce in the +4 state and substituting in the Ca and Zr sites respectively if single phases formed.

Ce-1 was found to be essentially single-phase zirconolite from XRD and SEM studies. Thus it was concluded that coupled substitution of $Ce^{+3} + Al^{3+}$ for $Ca^{2+} + Zr^{4+}$ allows Ce^{3+} to enter into Ca site. Further X-ray absorption spectroscopy however showed that this was so, only under reducing conditions. When the processing atmosphere was air, the Ce was approximately equally divided into the +3 and +4 states. This discrepancy is under further investigation by positron annihilation studies and TEM.

Sample Ce-2 contained alumina in addition to zirconolite and Ce-3 contained two zirconolites, one of which was relatively low in Ce and the other (possibly a pyrochlore) was relatively enriched in Ce. It is concluded that perhaps some, but certainly not all, of the Ce substituted as per the requirements of Ce-2 and Ce-3. Indeed our results for Ce-3 were similar to earlier results by Clinard for an analogous Pu-doped composition [13]. A set of samples of composition $Ca_{(x)}Ce_{(1-x)}ZrTi_{(2-x)}Al_{(x)}O_7$ gave XRD results which were broadly similar to the analogous Nd-doped series described above and implied extensive solid solubility of Ce^{3+} (and Ce^{4+}?) in the Ca site of zirconolite.

4.2.2 Radioactive specimens

Uranium. Our syntheses were designed to facilitate either (a) U^{4+} substituting on the Zr site, i.e. of formula or (b) U^{4+} substituting in the Ca site, along with two Al ions substituted on the Ti site for required charge compensation, giving a nominal formula of:

$$Ca_{(1-x)}U_{(x)}ZrAl_{(2x)}Ti_{(2-2x)}O_7.$$

The samples of nominal composition $CaZr_{(1-x)}U_{(x)}Ti_2O_7$ showed that the transformation from the zirconolite structure to pyrochlore occurred at an x value of around 0.5 with equilibration being assisted by short (≈ 2 hours) heat-treatments at 1300°C after hot-pressing, to remove metastable perovskite etc. However it was found that prolonged heating (for about 20 h) caused severe disproportionation. This was not investigated in detail however as the effect appeared to be present only at temperatures/times well outside reasonable limits for Synroc hot-consolidation.

The other suite of samples did not display such effects on heating in the 1300-1400°C range and it was concluded that the limits of U^{4+} solubility in the Ca site of zirconolite corresponded to x = 0.3-0.4. Extra phases observed at x >0.4 were mainly UO_2-ZrO_2 solid solutions and alumina.

Neptunium and Plutonium. The sample compositions and targeted actinide valencies are described in Table 4.2.1 and the XRD and SEM results are summarised in Table 4.2.2. (Guided by the results obtained for U-bearing samples we restricted high-temperature treatments after hot-pressing to short times at 1300°C to avoid possible disproportionation effects.) Nearly single phase zirconolites with the nominal formula given below were successfully synthesised, demonstrating the flexibility of the zirconolite structure to accommodate these nuclides in different sites by a variety of single and coupled solid solution mechanisms.

Table 4.2.1 Model valencies/site locations for Np and Pu in zirconolites.

Sample	Composition	Valence	Site
Np-1	$Ca_{0.8}Np_{0.2}ZrTi_{1.8}Al_{0.2}O_7$	+3	Ca
Np-2	$CaZr_{0.8}Np_{0.2}Ti_2O_7$	+4	Zr
Pu-1	$Ca_{0.8}Pu_{0.2}ZrTi_{1.8}Al_{0.2}O_7$	+3	Ca
Pu-2	$CaZr_{0.8}Pu_{0.2}Ti_2O_7$	+4	Zr

Table 4.2.2 Phase assemblages from XRD and SEM for hot-pressed Np- and Pu-doped zirconolites, before and after heat-treatment.

Sample	Heat-treatment	(wt%)				
		Zirconolite	"Pyrochlore"	Perovskite	Rutile	Zirconium
Np-1	-	100				
	H1	89			8	3
	H2	89			8	3
Np-2	-	80		20		
	H1	93*	7	<1	<1	
	H2	93	7	<1	<1	
Pu-1	-	85		15		
	H1	100				
	H2	95		5		
Pu-2	-	70		30		
	H1	90	10		<1	
	H2	88	7		5	

H1 and H2= 2 h at 1300°C in air or nitrogen respectively.
* Small peak observed at d spacing of 2.84 ± 0.01 A, very similar to the result obtained for Ce-3 above

The key conclusion from the XRD results was that, given the >90% abundance of zirconolite in all the heated samples, that both trivalent and tetravalent Np and Pu are readily accommodated under standard fabrication conditions.

In the Np-2 and Pu-2, Al-free formulations, SEM analyses of the zirconolites show that Np and Pu contents are less than those of the model compositions. These zirconolites coexist with a significant fraction of a more actinide rich pyrochlore-like phase. These results indicate that the solubility limits for Np and Pu have been exceeded, just as for the analogous Ce-3 sample mentioned above. Thus the Np and Pu species can only be incorporated to a maximum of about 0.15 to 0.17 cations per formula unit. In contrast, zirconolites in the Al-bearing Np-1 and Pu-1 formulations, phase assemblages and compositions are the same whether they were heated in air or nitrogen, while nitrogen favours the entry of Pu into the Ca site in the presence of charge-balancing aluminium.

TEM studies of Np-2 gave results in excellent agreement with the corresponding SEM studies, and the high-resolution lattice images showed the zirconolite crystallites (2M polytype) to be almost free of defects.

Key results are shown in Table 4.2.3. Experiments will be undertaken at the Stanford synchrotron facility in December, 1995 to confirm the conclusion about actinide valence states directly by X-ray absorption spectroscopy.

Table 4.2.3 Solid solubility (formula units) limits of REE + actinides in zirconolite, deduced from XRD and SEM studies.

RE/Ac	Ca site	Zr site
Nd^{3+}	0.65	<0.2
Ce^{3+}	0.65	?
Ce^{4+}	? (small)	0.15
U^{4+}	~0.2	0.5
Pu^{3+}	0.4	? (small)
Pu^{4+}	? (small)	0.15
Np^{3+}	0.4	? (small)
Np^{4+}	? (small)	0.15

4.3 Fabrication of Cm-Doped Zirconolite

From the work carried out at ANSTO in developing a precursor for actinide-doped zirconolite (as detailed in section 4.2) a set of samples was prepared assuming the actinides in the Cm-source to be trivalent and to be incorporated in the calcium site via coupled substitution of Al^{3+} on a Ti^{4+}, i.e.;

$$Ca_{0.97512}An_{0.02488}ZrTi_{1.97512}Al_{0.02488}O_7$$

However, as explained for Cm-doped perovskite (see Section 3.2), this is an approximation to the true state of affairs because some Ti^{3+} could be stabilised, as a result of the reducing conditions imposed by the use of the graphite dies, displacing a small amount of Al^{3+}.

The Cm used in this study contained 37 mole% of ^{244}Cm, and 58 mole% of ^{240}Pu the daughter nuclide of ^{244}Cm on May 24, 1994. A 0.8403 g sample of the Cm was dissolved in 45 g of concentrated nitric acid (HNO_3 content 61%, density, 1.38 g. cm^3 with 0.1 cm^3 of hydrofluoric acid (HF content, 47%), and then 10 cm^3 of 0.1N nitric acid was added to decrease the loss of the Cm source during subsequent processing. The Cm source was mixed with 41.6 g (oxide equivalent) of slurry precursor that consisted of 0.12027, 0.12341, 0.00314 and 0.24368 moles of calcium, zirconium, aluminium, and titanium, respectively, which was originally intended to incorporate 0.8589 g of the Cm source

The pH of the slurry mixture was adjusted to 9 with ammonium hydroxide. The slurry mixture was then poured into an in-cell calciner pot, dried at 80°C, and then calcined at 750°C for 2 hours in a stream of air. The powder, 41.0794 g, was collected from the calciner pot (recovery was 96.9%). The pour and tap densities of the calcined powder were measured before dividing it into three portions; 13.6998, 13.5457, and 13.8666 g, then each portion was hot-pressed using a graphite die at 1200°C and 29 MPa for 2 hours in a stream of N_2 gas.

4.4 Physical Properties of Cm-Doped Zirconolite-Rich Synroc

Pour and tap densities of the calcined powder were 0.62 (± 0.01) and 1.19 (± 0.01 $g.cm^{-3}$). The values in parentheses represent the standard deviation from seven measurements. The change in density of the Cm-doped zirconolite cylinder is shown on Figure 4.4.1 together with data from Cm-doped Synroc containing Na-free (PW-4b) and Na-bearing simulated high-level waste, and Cm-doped perovskite. The density changes are well fitted by linear extrapolation. At a dose of 3 x 10^{17} α-decays.g^{-1}, the fractional density decrease of the Cm-doped zirconolite was 0.4%. In Figure 4.4.1 the slope of the fitted line for the Cm-doped zirconolite is perhaps slightly smaller than that for the Cm-doped perovskite. The data themselves agree reasonably well with those of Vernaz et al[5] on ^{238}Pu and ^{244}Cm-doped zirconolite.

Figure 4.4.2 shows an X-ray diffraction pattern from the Cm-doped zirconolite one day after hot-pressing (dose = 1.7 x 10^{15} α decays.g^{-1}). The Figure indicates that the sample consisted mainly of zirconolite; it did not contain the less durable perovskite phase. However X-ray patterns from some other areas of the sample revealed that a considerable amount of additional phases occurred, mainly rutile and zirconia.

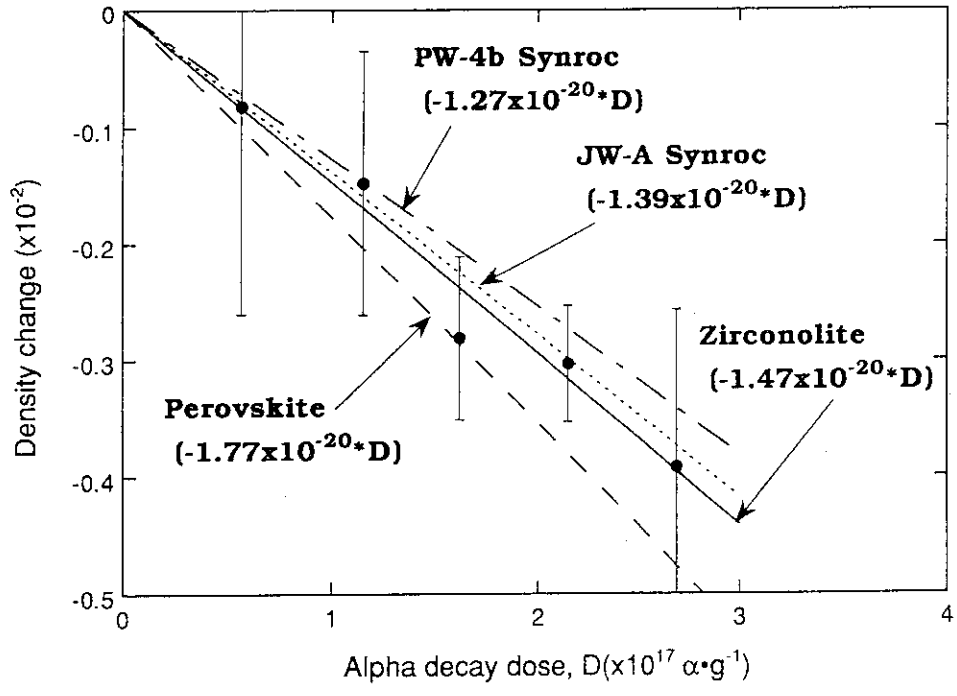

Figure 4.4.1 Change in density as a function of α-decay dose for Cm-doped Synroc containing JW-A and PW-4b waste, Cm-doped zirconolite and Cm-doped perovskite.

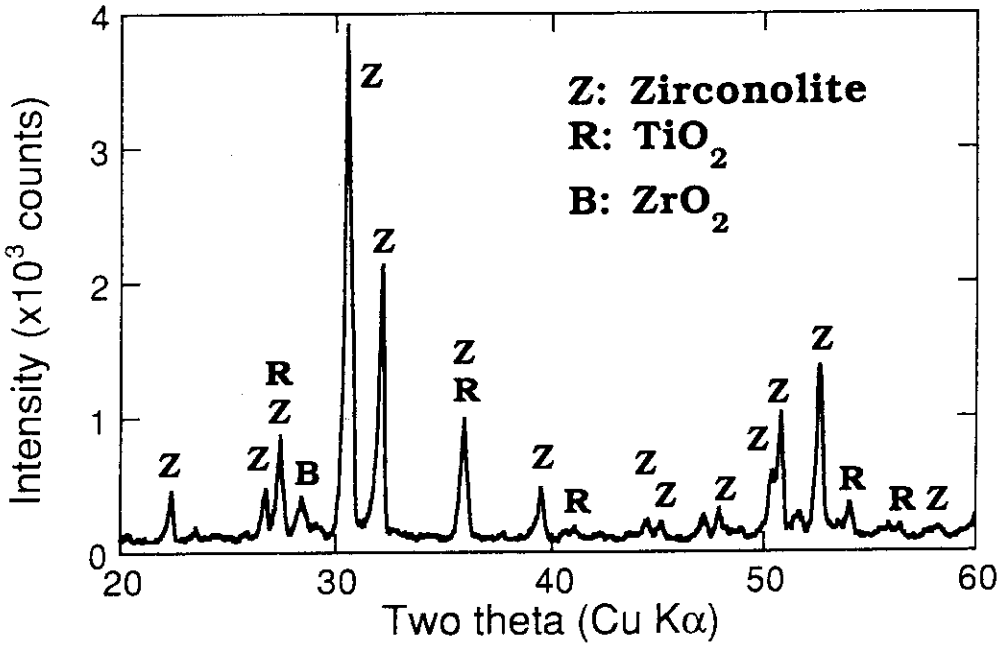

Figure 4.4.2 XRD pattern for Cm-doped zirconolite (dose = 1.7 x 10^{15} α decays.g^{-1}).

4.5 Leaching Behaviour of Cm-Doped Zirconolite-Rich Synroc

Flat faces and peripheries of three hot-pressed cylinders were polished with 6-μm diamond paste and #600 grit abrasive paper, respectively. The Cm-doped zirconolite cylinders, Z94002 and Z94003 were sliced and then cut across their diameters to make half-disk specimens for leach testing. Two half-disk specimens that had accumulated a dose of 1.5x10^{17} α decays.g^{-1} were MCC-1 leach tested in pH ~ 2 solution (0.05M KCl + 0.013M HCl) at 90°C for two months over four 7-day followed by one 28-day leach periods. The leachate samples were analysed by γ-ray spectrometry for ^{244}Cm and ICP-AES for Ca.

The normalised leach rate results of ^{244}Cm, and changes in pH with time, are shown in Figure 4.5.1. This Figure also shows a comparison between zirconolite and perovskite over similar leaching conditions. The leach rates of the two materials are different at late stages of the first month, but similar in the final leaching run due to the lower Cm solubility at the higher pH of the perovskite leachate.

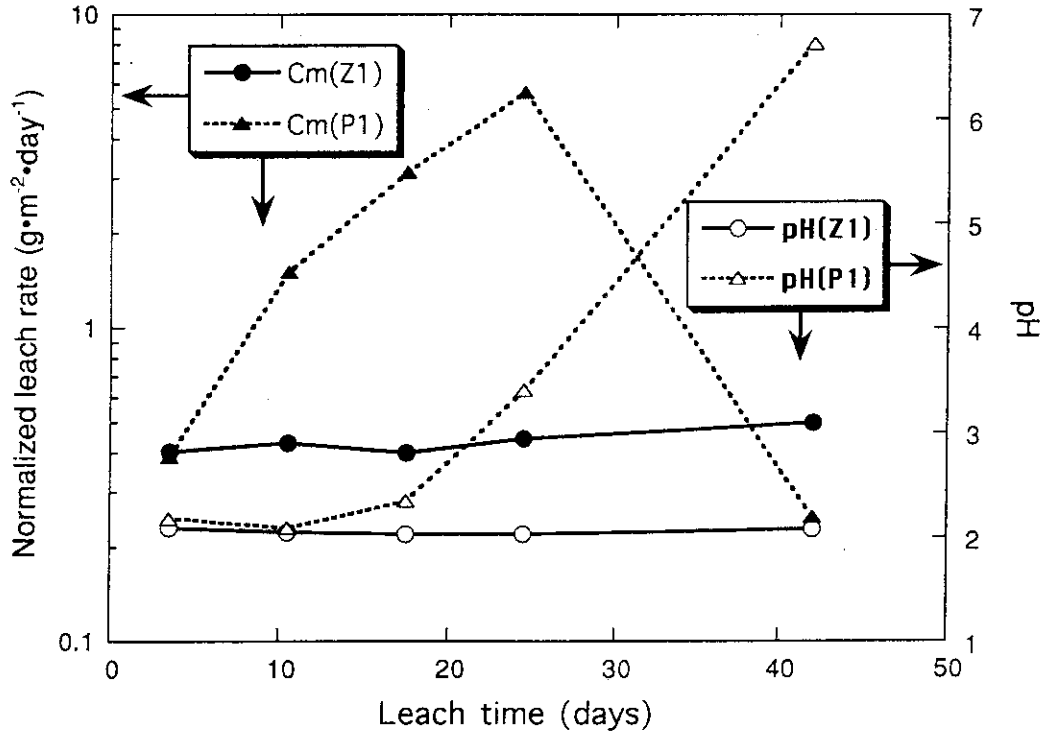

Figure 4.5.1 Normalised leach rate of ^{244}Cm and pH versus leach time. (Z1 & P1 stand for Cm-doped zirconolite and perovskite, respectively.)

4.6 Development of Zirconolite-Rich Ceramics for Immobilisation of Partitioned Reprocessing Waste Actinides

For partitioned actinide-rich reprocessing wastes, we have aimed at a ceramic composed of ≈ 80 wt% zirconolite, plus ≈ 5 wt% each of hollandite, perovskite and rutile. In this work we have assumed that U will be tetravalent, and that other actinides can exist as trivalent species on the Ca site of zirconolite. We have used Nd^{3+} as a simulant of such trivalent actinides and have added U as necessary. In early work, we tried to achieve a waste loading of 30 wt% of an equimolar mixture of Nd and U, but pyrochlore formed instead of zirconolite. Also, considerable amounts of brannerite (UTi_2O_6) formed. We decreased the target waste loading to 20 wt%. In our phase design, we have somewhat arbitrarily used an equimolar mixture of +4 and +3 waste actinide ions, corresponding to a reprocessing efficiency of > 99%.

The composition of the zirconolite-rich ceramic was (wt%): Al_2O_3 (2.6); BaO (2.4); CaO (10.0); Nd_2O_3 (6.6); TiO_2 (48.4); UO_2 (10.4); and ZrO_2 (19.6). It was hot-pressed at 1170°C/20 MPa. The desired phase assemblage was obtained from XRD studies, although traces of brannerite were still observed. The compositional flexibility of this ceramic was such that little change of phase assemblage occurred when the waste loading was varied between 16 and 24 wt%.

Leaching experiments were carried out on these samples, plus the above mentioned samples with 30 wt% loading. After periods of 7 and 28 days, the total (vessel wall + solution) elemental extractions agreed within an order of magnitude and lay in the ranges of (g m^{-2} d^{-1} at 90°C): 10^{-1} to 10^{-2} (Ca); 10^{-2} to 10^{-3} (Ba); 10^{-3} to 10^{-4} (Nd); 10^{-2} (Al); 10^{-4} to 10^{-5} (U); 10^{-6} (Ti); and 10^{-7} (Zr). The leach rates decreased with time, and were comparable with equivalent values for reference-grade Synroc-C. Further work will utilise U, Np and Pu as waste elements.

Leach rates from Cm-doped samples are higher than those obtained for comparable 'cold' samples. This will be investigated further in the extension to the Phase II program.

5. FUNDAMENTAL STUDIES OF TRU IMMOBILISATION MECHANISMS

5.1 Background

The ability of the Synroc matrix to contain TRU elements has been mostly demonstrated in short-term (1-100 days) leaching studies, but in order to extrapolate these results to the performance of the waste form under repository conditions over geological time, it is necessary to be able to understand and model the leaching behaviour of Synroc. The short-term leaching effort has consisted of surface studies via microscopy and secondary ion mass spectrometry (SIMS), leaching studies of nominally single-phase powders, extended (>200 days) leaching studies and studies of natural analogues of Synroc phases. The results of these studies are explained and interpreted where possible below.

5.2 Surface Studies

5.2.1 SIMS

Two monoliths of Synroc have been tested in-situ in the HADES facility at Mol for 3.5 years at 90°C in contact with the clay. These samples were weighed before and after these tests to determine the mass loss and analysed by SIMS by Prof Lodding (Chalmers University of Technology, Sweden). The weight changes were difficult to interpret, as although one sample had lost ≈ 1 % of its weight the other had gained a comparable amount. SIMS analysis (one analysis is shown in Figure 5.2.1) shows that alteration of the matrix occurred to depths of about 0.25 for one sample and 0.35 μm for the other. The Synroc matrix elements appear to have been released congruently with counter-diffusion of elements arising from the clay into the matrix through the altered layer, suggesting that this layer is to a certain extent porous. The very thin alteration layers on these specimens makes it very difficult to study them and to draw significant conclusions on their effect on the mechanisms of leaching and the release of elements from Synroc.

Leaching experiments were carried out on these samples, plus the above mentioned samples with 30 wt% loading. After periods of 7 and 28 days, the total (vessel wall + solution) elemental extractions agreed within an order of magnitude and lay in the ranges of (g m^{-2} d^{-1} at 90°C): 10^{-1} to 10^{-2} (Ca); 10^{-2} to 10^{-3} (Ba); 10^{-3} to 10^{-4} (Nd); 10^{-2} (Al); 10^{-4} to 10^{-5} (U); 10^{-6} (Ti); and 10^{-7} (Zr). The leach rates decreased with time, and were comparable with equivalent values for reference-grade Synroc-C. Further work will utilise U, Np and Pu as waste elements.

Leach rates from Cm-doped samples are higher than those obtained for comparable 'cold' samples. This will be investigated further in the extension to the Phase II program.

5. FUNDAMENTAL STUDIES OF TRU IMMOBILISATION MECHANISMS

5.1 Background

The ability of the Synroc matrix to contain TRU elements has been mostly demonstrated in short-term (1-100 days) leaching studies, but in order to extrapolate these results to the performance of the waste form under repository conditions over geological time, it is necessary to be able to understand and model the leaching behaviour of Synroc. The short-term leaching effort has consisted of surface studies via microscopy and secondary ion mass spectrometry (SIMS), leaching studies of nominally single-phase powders, extended (>200 days) leaching studies and studies of natural analogues of Synroc phases. The results of these studies are explained and interpreted where possible below.

5.2 Surface Studies

5.2.1 SIMS

Two monoliths of Synroc have been tested in-situ in the HADES facility at Mol for 3.5 years at 90°C in contact with the clay. These samples were weighed before and after these tests to determine the mass loss and analysed by SIMS by Prof Lodding (Chalmers University of Technology, Sweden). The weight changes were difficult to interpret, as although one sample had lost ≈ 1 % of its weight the other had gained a comparable amount. SIMS analysis (one analysis is shown in Figure 5.2.1) shows that alteration of the matrix occurred to depths of about 0.25 for one sample and 0.35 μm for the other. The Synroc matrix elements appear to have been released congruently with counter-diffusion of elements arising from the clay into the matrix through the altered layer, suggesting that this layer is to a certain extent porous. The very thin alteration layers on these specimens makes it very difficult to study them and to draw significant conclusions on their effect on the mechanisms of leaching and the release of elements from Synroc.

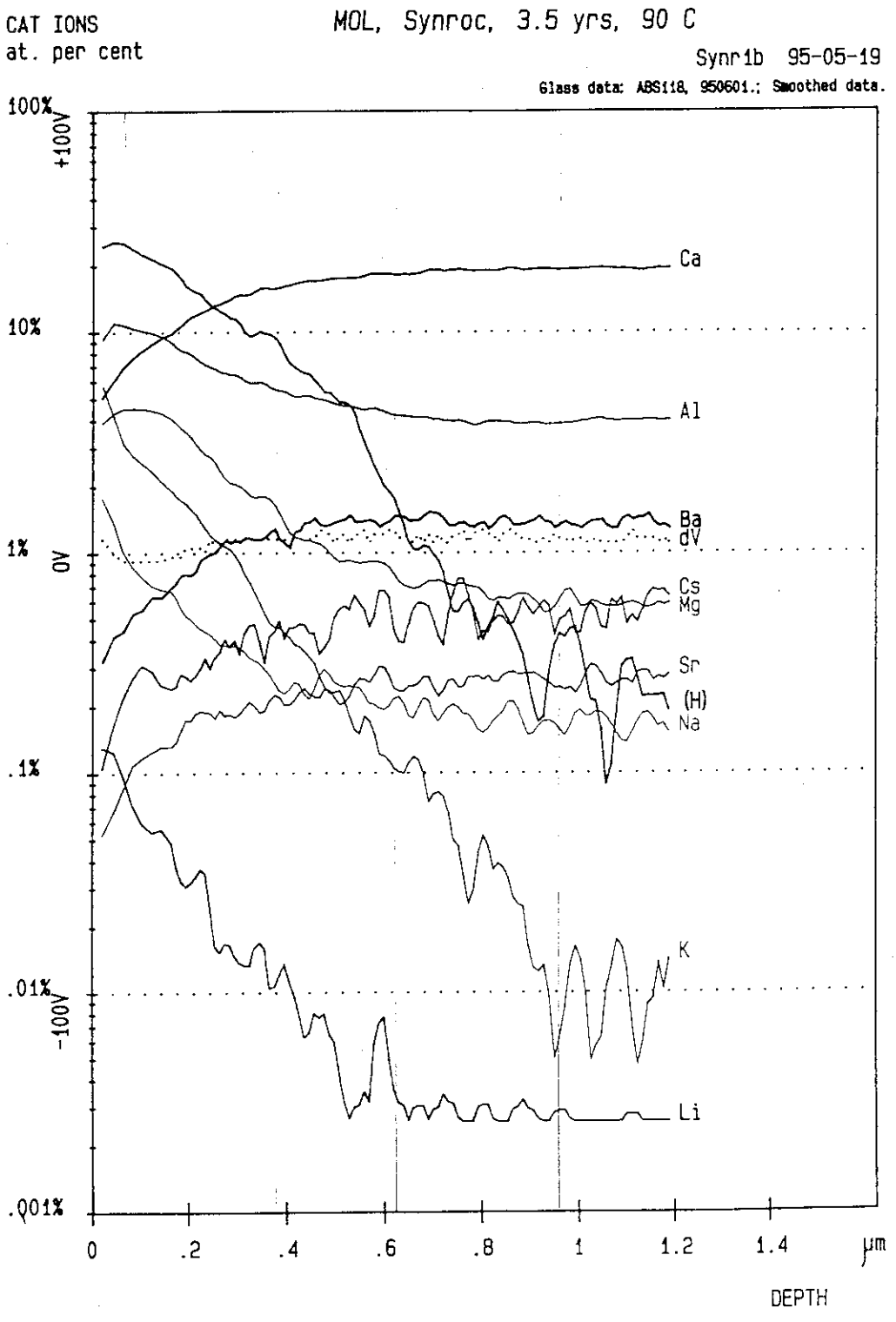

Figure 5.2.1 Depth profile, measured by SIMS, for a Synroc specimen leached for 3.5 years in-situ in the HADES facility at 90°C in contact with the clay.

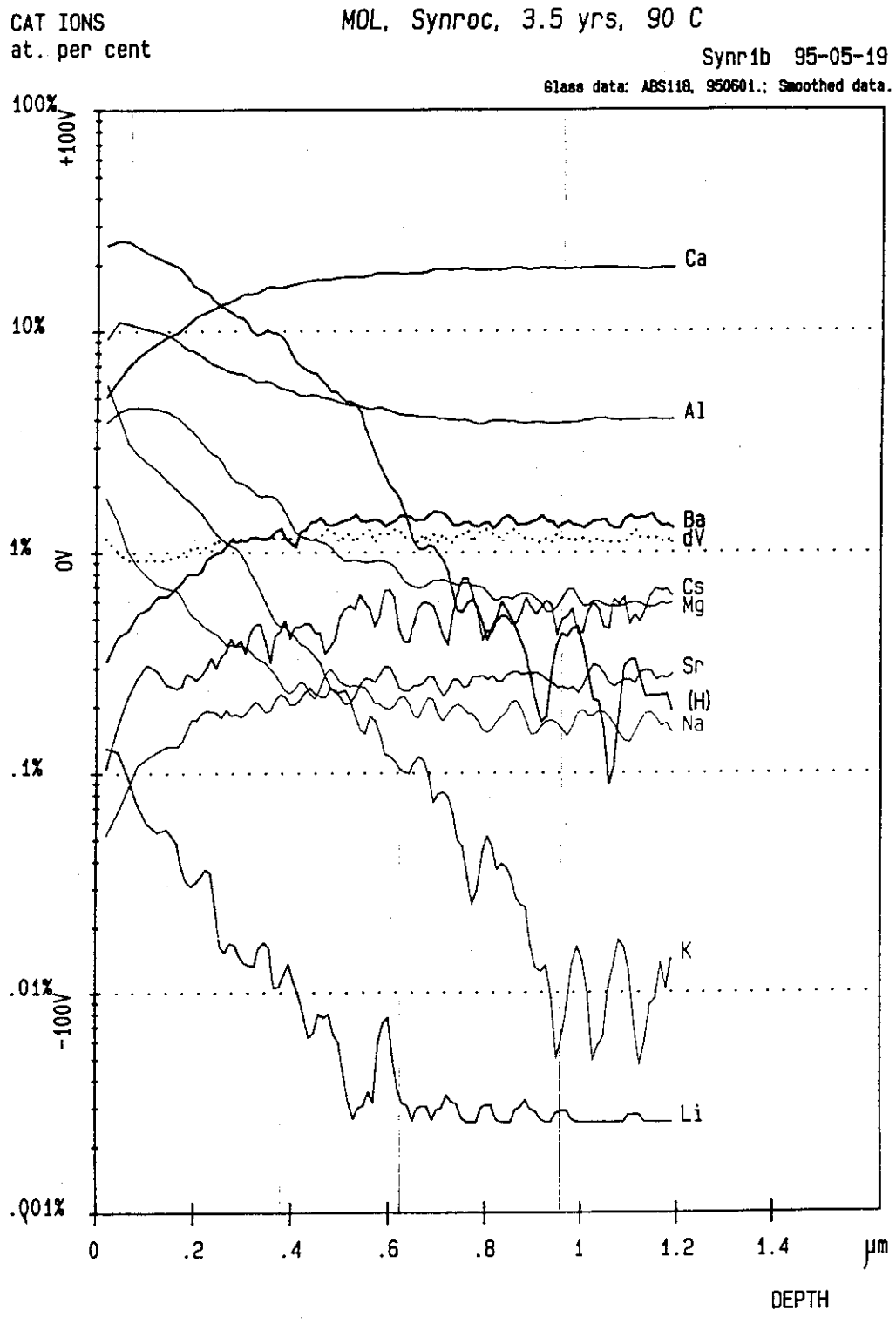

Figure 5.2.1 Depth profile, measured by SIMS, for a Synroc specimen leached for 3.5 years in-situ in the HADES facility at 90°C in contact with the clay.

5.2.2 Microscopy Studies

Work on the alteration of Synroc leached at 70°C in deionised water and some synthetic ground water solutions was reported in the Phase I report. This work has been expanded on in Lumpkin et al [16] where secondary phases have been identified on the surface of Synroc specimens, containing simulated PW-4b HLW, that were leached in deionised water for periods up to 532 days at 150°C. Analytical electron microscopy (AEM) was used as the principal tool for this study because of the fine-grained nature of the alteration products and the high durability of the Synroc matrix. The major findings of this study are given below.

After 532 days of leaching at 150°C the surface of the Synroc specimens was not totally covered by secondary phases (see Figure 5.2.2). Only perovskite, minor Al-rich oxides and intermetallic phases occurred on the Synroc surface, most of which were quite low in abundance. Crystalline polymorphs of TiO_2 were the major secondary phases developed on Synroc after exposure to deionised water at 150°C, mainly forming as a result of the dissolution of perovskite. Most of the perovskites grains underwent a rapid initial release of Ca, Sr and REE cations, followed by crystallisation of a fine-grained, low-porosity layer of anatase. Although this layer appears to partly protect the underlying perovskite from further dissolution, further interaction with the fluid phase was indicated by slow grain growth and development of epitaxy at the perovskite-anatase interface. However, other perovskite grain orientations yielded numerous individual crystals of brookite which exhibited pronounced growth with time but even so, some of the underlying perovskite surfaces remain partially exposed to the leachant. The low rate of alteration at 150°C even with surface phases apparently unprotected by surface layers or secondary phases suggest that the roles played by surface hydrolysis, ion exchange and other processes during the alteration of perovskite at 150°C are not well established and require investigation by other techniques.

AEM and SEM studies have also been carried out on Np-doped specimens of Synroc that had been leached in deionised water at 70°C for varying periods of time[3]. The results of this study have shown that after 56 days of leaching there are secondary phases on the surface of the specimen, but they are mainly associated with polishing scratches and perovskite (see Figure 5.2.3). After 400 days of leaching the surface was almost covered and as the leaching time was further increased up to 2283 days the surface of the specimens slowly became covered in secondary phases. However the polishing scratches still were not completely filled in (see Figure 5.2.3). Replica samples of the secondary phases have been studied by AEM. The surface phases that were sampled by this technique, which tends to remove only the least adherent alteration phases and is not a quantitative sampling method, were found to be crystalline and have been identified as anatase, brookite and ilmenite. Importantly, no phases incorporating Np have been identified on the surface of the sample.

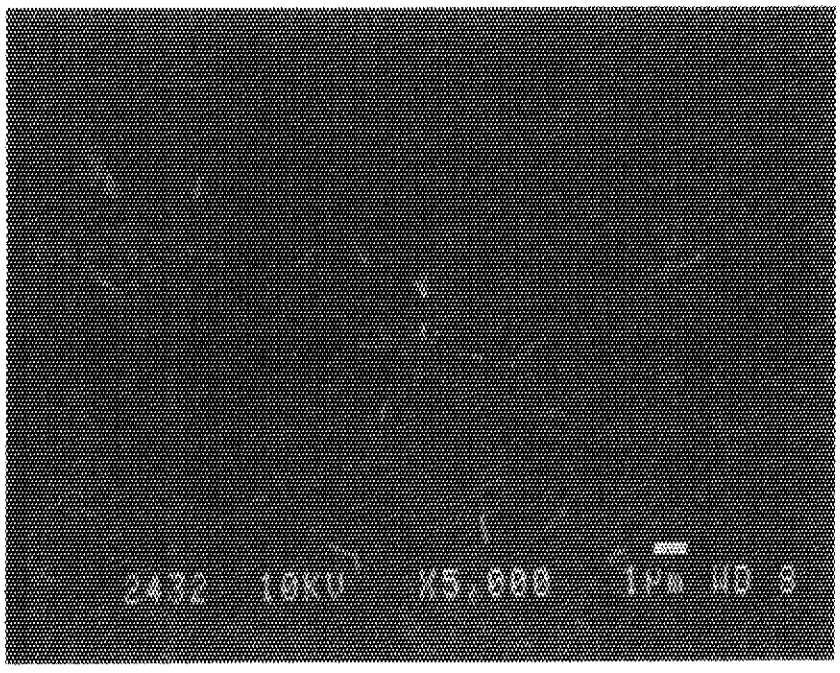

Figure 5.2.2 Formation of secondary phases on the surface of Synroc after leaching in deionised water for a total of 532 days at 150°C.

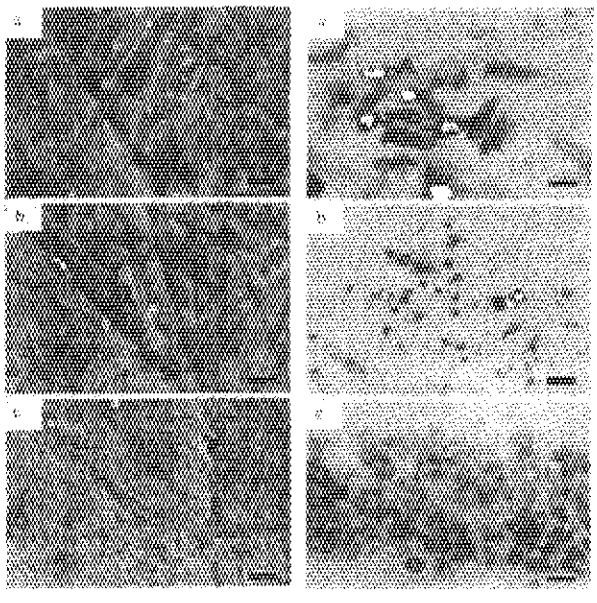

Figure 5.2.3 (1) surfaces of leached Np-doped Synroc disks after (a) 56 days, (b) 422 days and (c) 2283 days. Scale bar is 1 μm in all photographs and (2) Secondary Ti-oxide phases on replicas from leached Np-doped Synroc disks (a) anatase crystals, (b) brookite crystals and (c) ilmenite crystals. Scale bar is 100 nm in all photographs.

The secondary phases seen on the Np-doped Synroc are different from those seen on inactive samples leached at the same temperature, with some secondary ilmenite being present on the actinide-doped samples. This may be due to the difficulties of preparing the samples in the glove box where less efficient mixing is used. SEM examination of the surface of actinide-doped Synroc has shown that there are some areas of Fe-segregation on the surface and the relatively faster leach rates of these segregations may have provided enough of this element to enable ilmenite to form on the surface.

The results from the microscopy studies of Synroc, both undoped and doped with actinides, and leached at 70°C and 150°C, emphasise the very slow reaction of this material. This of course gives rise to difficulties in developing a full description of the leaching mechanisms.

5.3 Leaching Studies

Studies of Synroc dissolution under repository conditions are being undertaken for times which are as long as possible, so that real-time data can then be extrapolated on chemically defensible grounds to satisfactorily predict behaviour in a repository over periods of at least 10^4 years. Part of this task requires kinetic data for the leaching of individual phases that make up Synroc. Recent results from the leaching of the single phases and the long-term data for ^{134}Cs are reported below together with an interpretation of the types of mechanisms that can account for the releases that are occurring form the phases being studied.

5.3.1 Long-term leaching studies

The slow reaction rate of monolithic Synroc with solutions can be dealt with in laboratory experiments to a certain extent by utilising powdered samples. Work reported previously[17] and results obtained by Van Iseghem[18] have shown at high SA/V ratios(using powders) that the overall releases from Synroc are dominated by initial releases, i.e. those occurring over the first day, with relatively little further dissolution occurring with increasing time. At SA/V ratios greater than 1,000 there is a decrease in the solution release rates of Mo, Ba and Ca, consistent with precipitation of these elements.

Another approach has been to use powdered specimens of the individual Synroc phases to determine the dissolution kinetics. Perovskite ($CaTiO_3$), doped perovskite ($(Ca_{0.78}Sr_{0.04}Nd_{0.18})Ti_{0.82}Al_{0.18}O_3$) and zirconolite ($CaZrTi_2O_7$) samples have been studied under flow-through conditions (~ 30 mL d^{-1}, for perovskite and ~ 3 mL d^{-1} for zirconolite) in pH-buffered leachants (pHs 2.1, 3.5, 6.1, 7.8, 10.4 and 12.8) at 90°C . Very small solid samples (≈ 0.1 g) and flow-through conditions were used to avoid saturation and other effects

that may mask the kinetics and mechanisms of leaching. Initial results of this study have been reported elsewhere[19], additional results have been obtained which have extended and elaborated upon these initial results.

Figure 5.3.1 shows the release of Ca at different pHs from the powders after 43 and 192 days of leaching. The data for 43 days of leaching (see Figure 5.3.1(a)) show that there is a decrease in release of Ca from zirconolite and perovskite with increasing pH in the range from 2 to 13. The releases from the perovskite and doped perovskite are generally similar except for the pH = 2.1 experiments. The release of Ca from zirconolite is a factor of three less than that for the perovskite and the doped perovskite samples at pHs ≤ 6 but approaches similar levels under alkaline conditions. The release of Ca into solution varies by less than a factor of 10 over the pH range 2.1 to 12.9, i.e. for hydrogen ion activity varying by nearly 11 orders of magnitude.

After 192 days of leaching (see Figure 5.3.1(b)), Ca release in the pH = 2 buffer from the perovskite samples is higher than that measured for 43 days, by a factor of between 2 and 5, whereas at the other pHs the amount released has changed very little from the 43 day releases. Ca release from zirconolite for up to 192 days shows no significant dependence on pH.

At all pHs the release of Ca far exceeds that of Ti (see Figure 5.3.2). At neutral pHs the ratio is the greatest, probably because of the formation of highly insoluble titanium species. Examination of the leached powders, using SEM/EDS and XRD, has established the presence of anatase and rutile on the perovskite surface (see Section 5.2.2). This result is consistent with the work of Pham et al[20]. These authors suggested that the dissolution of perovskite, at temperatures ≤ 90°C, in deionised water could be described by the following equation;

$$CaTiO_3 + (6-x)H^+_{(aq)} \leftrightarrow Ti(OH)_x^{(4-x)+} + Ca^{2+}_{(aq)} + (3-x)H_2O \qquad (1)$$

Temperatures > 90°C facilitated the decomposition of the titanium hydroxides, followed by the nucleation and growth of TiO_2 crystals. The presence of anatase and rutile on some of the leached perovskite and doped perovskite specimens in this study suggests that this mechanism may be operating here, as the experimental temperature was close to 90°C.

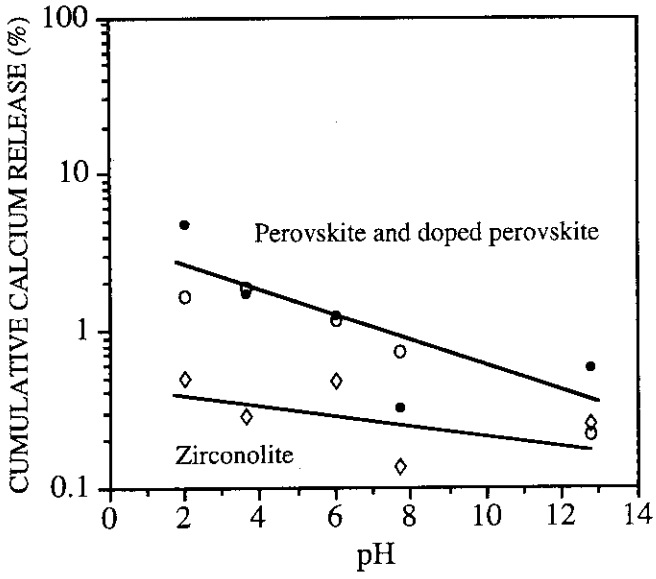

(a)

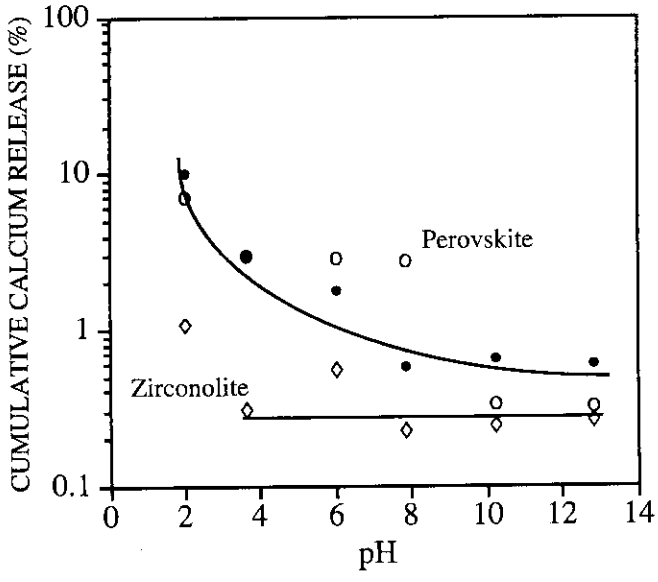

(b)

Figure 5.3.1 Cumulative Ca release from doped perovskite, perovskite and zirconolite at different pHs after (a) 43 days and (b) 192 days of leaching at 90°C.

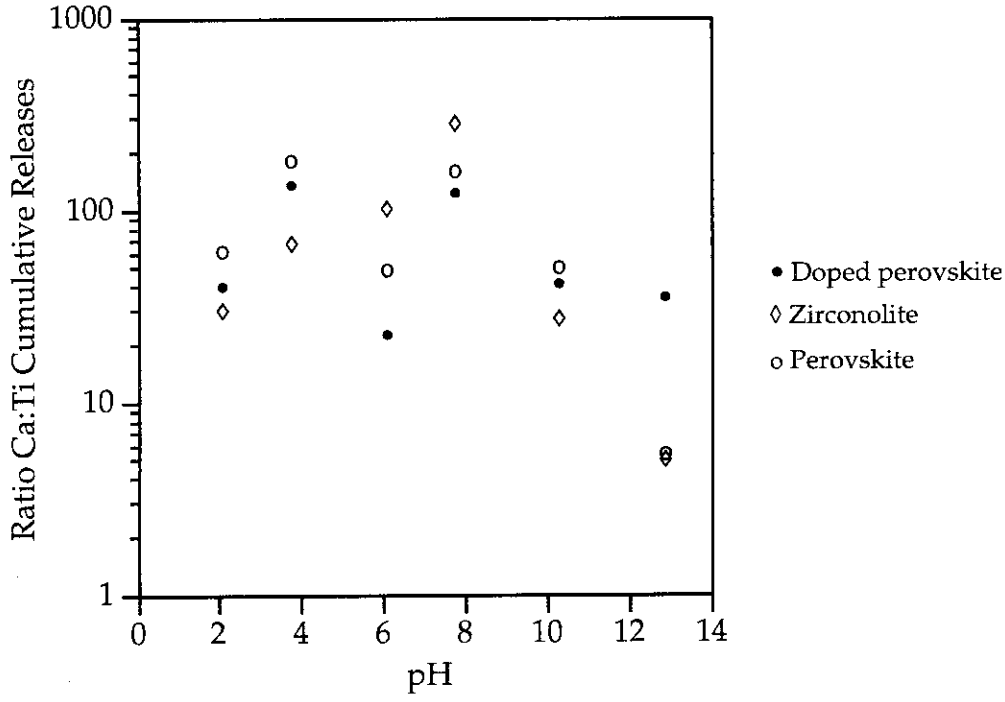

Figure 5.3.2 Effect of pH on the relative release of Ca to Ti from single phase, powder samples.

Equation (1) describes a leaching mechanism which is strongly dependent on pH; however our studies show that there is not a strong effect of pH on Ca or Ti releases and that the kinetics of leaching change with time. Generally, the initial release of Ca is rapid at all pHs but after this instantaneous release, the rates of release drop off markedly. So although the reaction may proceed in the very short term, i.e. < 1 day, as described by the above equation, the longer-term release of Ca is evidently controlled by other processes.

Leaching studies of zirconolite have shown that releases of Ca also appeared to be only weakly dependent on pH. The slow reaction rate of the zirconolite makes it difficult to quantify the leaching mechanisms but as Ca is released into solution in much larger quantities than Ti and Zr, it appears that similar processes like those for perovskite also control releases from zirconolite. Lack of any SEM evidence for the presence of secondary phases on the zirconolite powders does not allow any conclusions to be made about zirconolite dissolution at this stage.

The data above for powdered samples are relatively long-term, with the shortest leach period being one day. To obtain initial reaction rates much shorter periods of time must be used. So studies for the first day of leaching have also been carried out on the perovskite powder sample. Figure 5.3.3 shows the releases of Ca with time for short leaching periods at pH 2.4 and 13.0. As expected the releases from the perovskite in pH = 2.4 buffer 40 times higher than at pH 13. But, the data show that the releases are proportional to time for only very short times, i.e. less than 2 hours at pH = 2.4 and less than 5 hours at pH = 13.

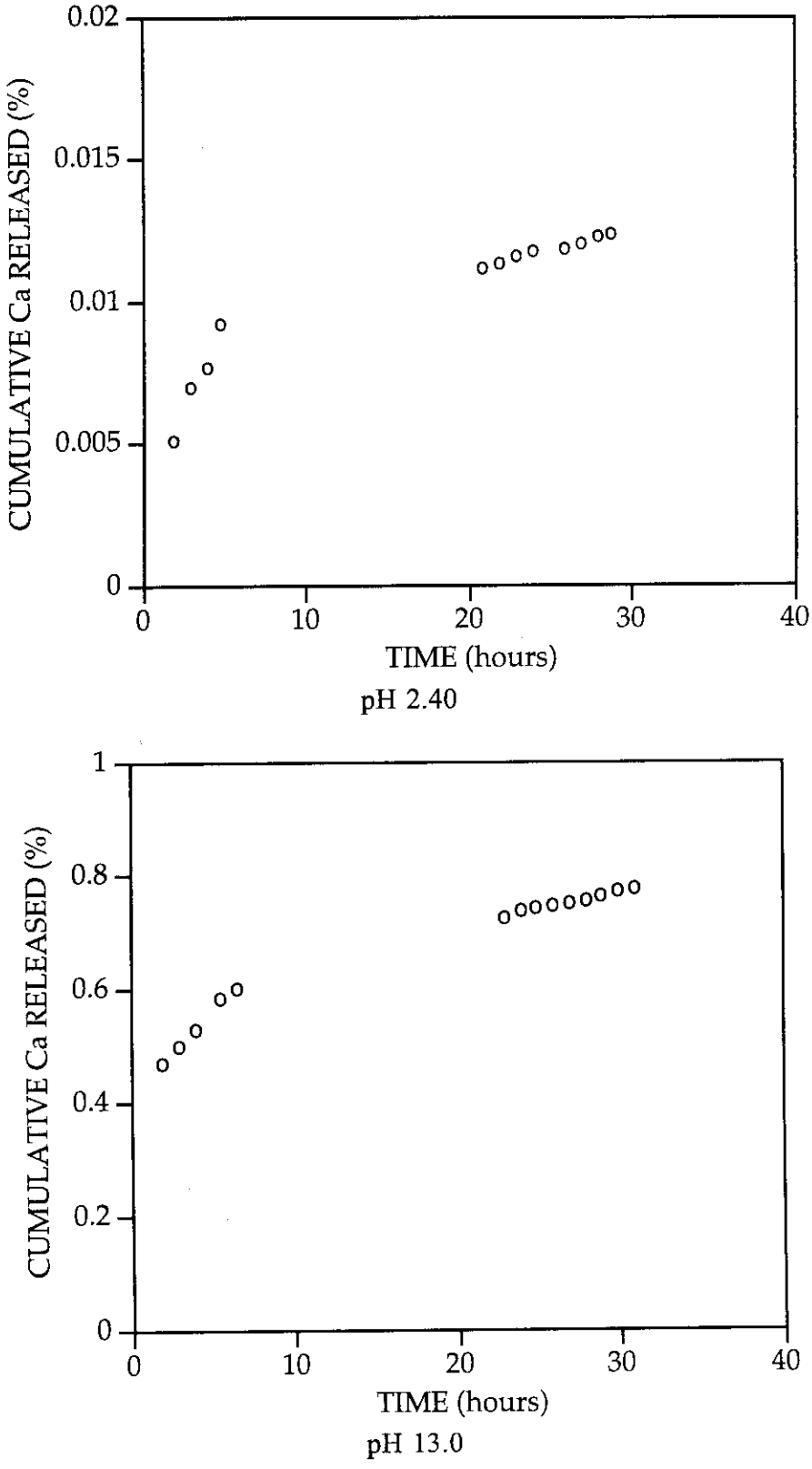

Figure 5.3.3 Ca releases from perovskite measured over short periods of time in pH 2.4 and 13.0 buffers at 90°C.

The results obtained for the perovskite powders are very similar to results obtained for pH controlled experiments carried out with Np-doped Synroc (see Figure 5.3.4), with the exception of the value measured at pH 2. The leach rate of Np is relatively unaffected by changing pH with leach rates varying by less than a factor of 10 over the pH range 5.4 to 10. From Figures 5.3.1 and 5.3.2 it can be seen that these pHs correspond to the regions where releases are lowest from the powders. However when the same studies were carried out with Synroc doped individually with Am, Pu, and Cm, the effect of pH was much greater (see Figure 5.3.4). The leach rates of Pu, Am and Cm were reduced by between 3 and 4 orders of magnitude and were lowest between pHs of 7 and 10, reflecting the reduced solubility of these elements under alkaline conditions.

These results emphasise that not only is the matrix important for controlling the release of elements but the chemistry of the element under the repository conditions must be well known to enable leaching processes to be coupled with reliable chemistry and transport codes. Currently, our ability to describe the behaviour of radionuclides like Pu, Am and especially Cm are limited by knowledge of their solution chemistry. Unlike the fission products where stable isotopes of most elements are available for study, a wide range of data for the actinide elements is not included in most thermodynamic databases.

Results from the leaching studies have established that, for both powdered samples and monoliths under static conditions, increasing the leaching time does not increase the release of elements from Synroc. Additionally the only phases identified on the surface of the leached specimens are Ti-rich and do not appear to incorporate fission products, ^{134}Cs, or actinides.

Additionally, the low releases appear to be associated with a very thin alteration layer, ~ 0.3 μm over 3.5 years at 90°C, which is appears to be somewhat permeable allowing the transport of matrix elements to the solution and elements in solution from the clay into the Synroc specimens. The driving force for this transport appears to the concentration gradient between the solid/liquid interface and the bulk solution.

These results suggested that if the releases from Synroc were to be modelled then calculations should be based on diffusion through an altered layer. This was checked in a simple manner initially by using a calculation based on the shrinking core approach[21] with releases from the core being assumed to be controlled by diffusion through an altered layer surrounding the core. The calculation was carried out by assuming the particles were spherical and then calculating the time taken to react the whole particle from the known conversion at a given time. This allowed the time taken to react the whole particle, given that the diffusion mechanism was controlling releases, to be calculated (see Table 5.3.1). The long times calculated to react small perovskite particles are in agreement with the experimental data which show that only very small releases of Ca have occurred under flow-through conditions.

From the calculated constants given in Table 5.3.1 the release of Ca as a function of time for each pH was calculated. Figure 5.3.5 shows the comparison between the calculated and experimental points. (It should be noted that not all of the experimental points are shown in this Figure.) With the exception of pH 2.1 and 7.8, there is excellent agreement between the predicted and measured Ca releases. At pH 2.1 the agreement is still reasonable but the calculated results for pH 7.8 are too high. The results shown in Figures 5.3.1 and 5.3.2 suggest that at this pH releases of Ca are low and may be affected by precipitation or by low Ca solubilities. Overall, the disagreements at pH 2.1 and 7.8 are minor given our very simple initial approach and the calculations strongly suggest that it is not possible to model Ca releases using a thermodynamic equilibrium approach but instead a model that allows transport by diffusion and other surface interaction processes to be included should be used.

The findings from the work with single-phase powder samples are in agreement with long-term leaching studies that have been carried out using Synroc doped with ^{134}Cs. These results (see Figure 5.3.6) show that the release of Cs per unit time drops rapidly with time even if the leachant is replaced regularly. The data plotted as a function of the square root of time are shown in Figure 5.3.7 and appear to show that as leaching time increases, the release is slowed by apparently thicker, and hence more retardant, layers on the surface of the monolithic samples.

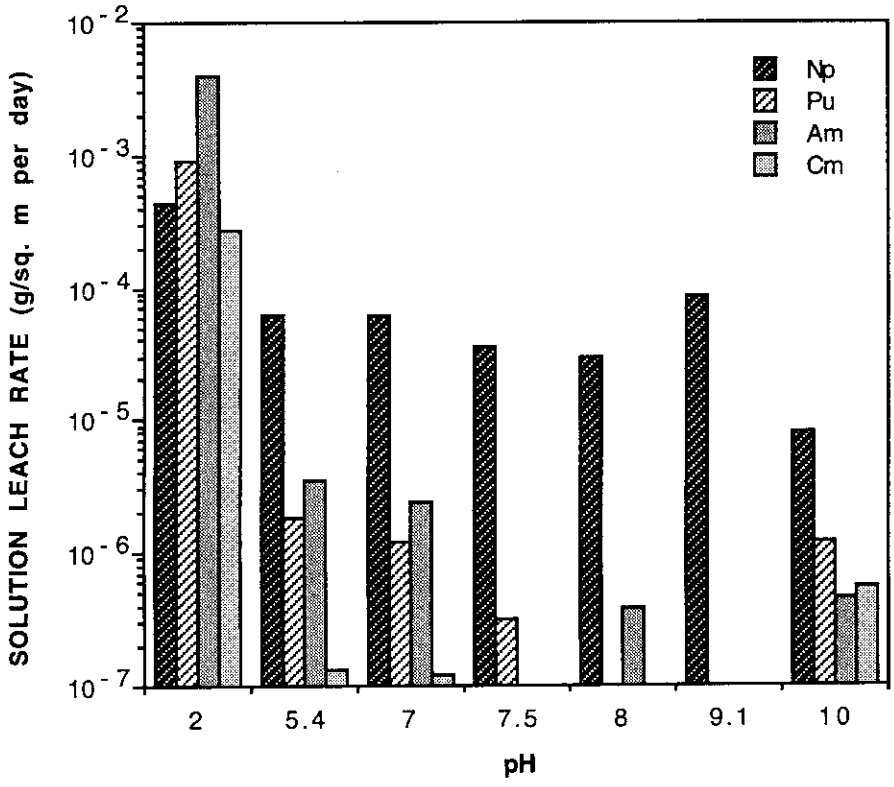

Figure 5.3.4 Effect of pH on the solution leach rate of Np, Pu, Am and Cm from Synroc (28 day leach tests at 70°C)

Table 5.3.1 Calculated time as a function of pH for complete dissolution (t) of perovskite, based on calcium release results at 90°C.

pH	t (years)
2.1	87,500
3.8	606,474
6.1	766,304
7.8	197,054
10.3	49,615,000
12.9	86,464,000

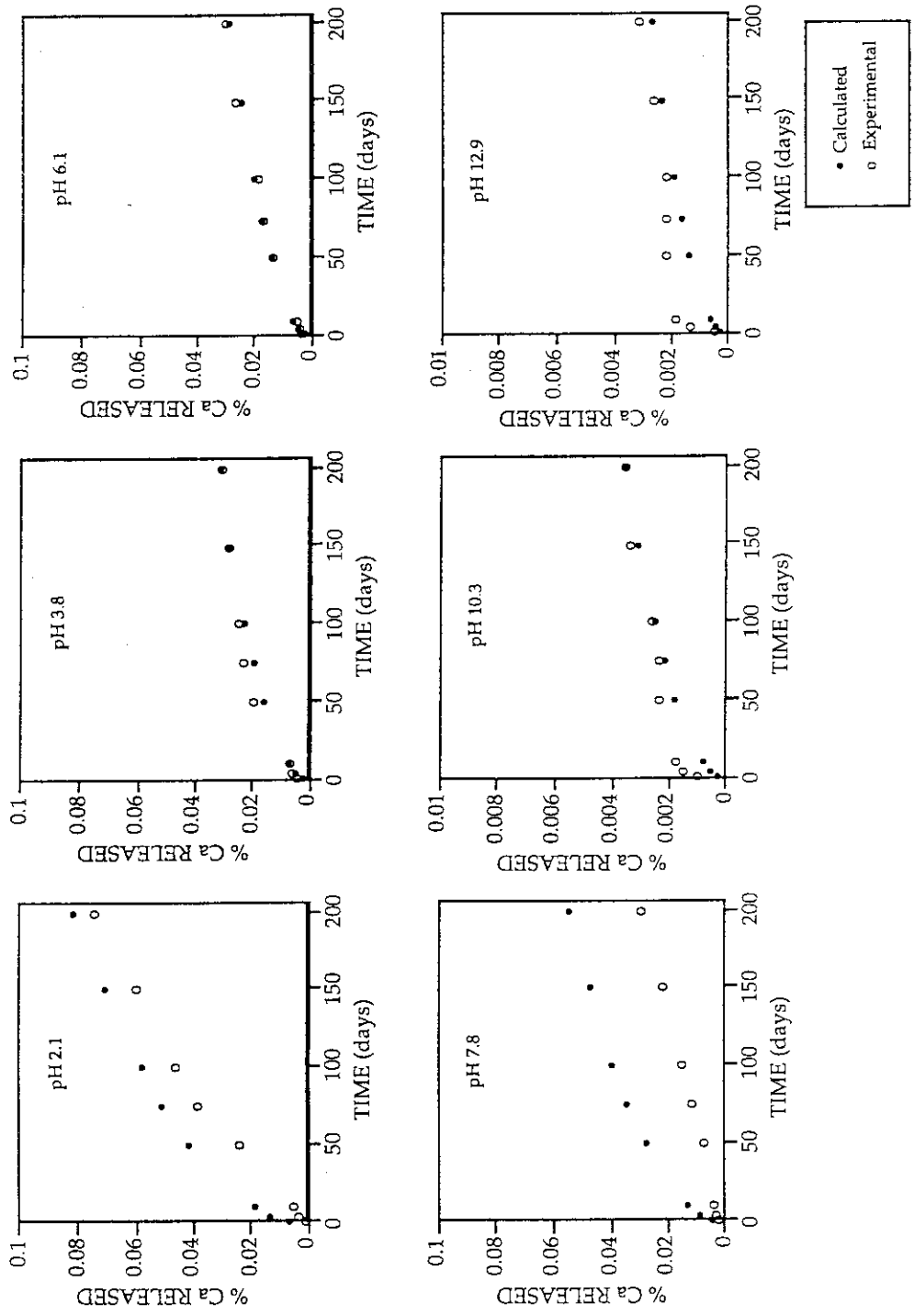

Figure 5.3.5 Comparison of calculated and measured cumulative releases of Ca from perovskite as a function of pH.

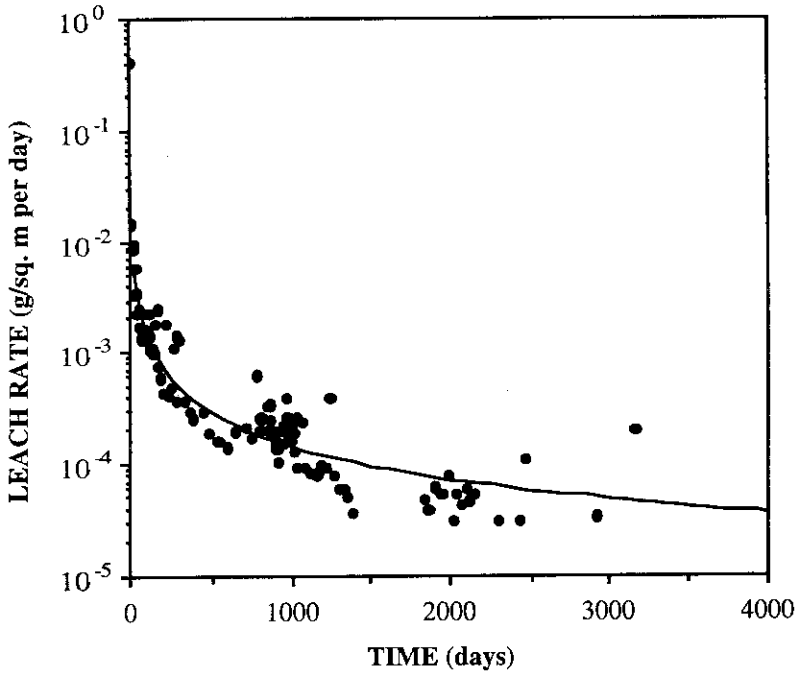

Figure 5.3.6 Long-term release of ^{134}Cs from Synroc leached in deionised water at 70^0C.

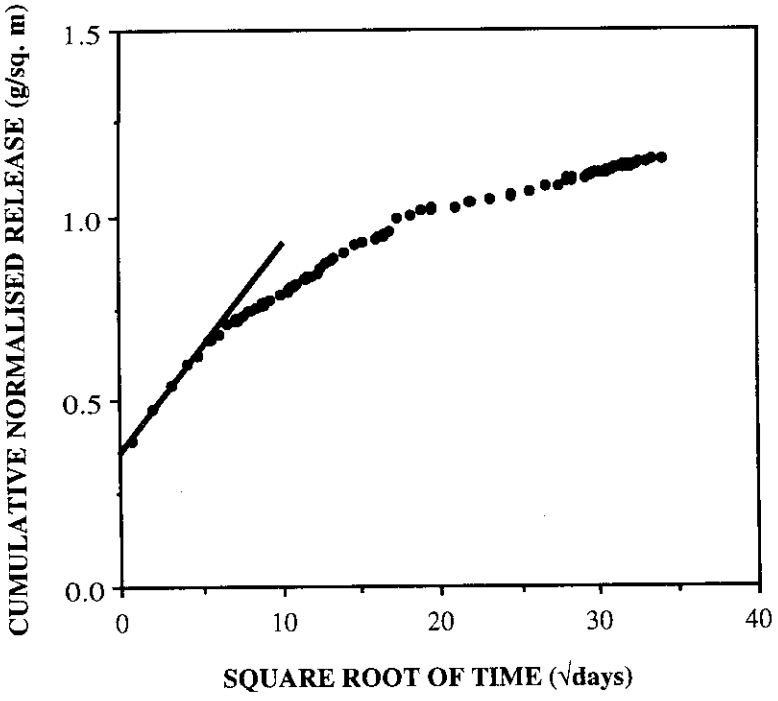

Figure 5.3.7 Cumulative ^{134}Cs release as a function of the square root of time (days).

5.4 Fundamental Studies using Natural Analogues of Synroc and Zirconolites

The overall objective of this section of the work is to investigate the stability, crystal chemistry, radiation damage effects, and geochemical alteration of natural analogues of Synroc phases, especially zirconolite, to provide information for long-term modelling of Synroc behaviour in the repository environment. As discussed earlier, zirconolite is the phase in Synroc which incorporates most of the actinide elements[22] and so it becomes of primary interest in studying the effects of α–decay damage on the retention of actinides in the wasteform over the life of the repository. Radiation damage effects and geochemical alteration are of even greater concern in the development and testing of zirconolite rich ceramics for disposal of weapons-grade Pu, and also other actinide waste schemes, for example Vance et al. [23]. Some specific objectives of the work, for example long-term annealing effects at ambient temperature, can only be addressed using natural samples. In other cases, natural analogue studies point to specific problems that can be addressed through complementary laboratory experiments, for example, identification of fluid compositions that may lead to the corrosion of zirconolite[24]. The philosophy of the current research program is to adopt a multidisciplinary approach to problem solving. Currently we employ SEM, TEM, ICP-MS, and α–spectrometry at ANSTO in collaboration with Dr. R. Gieré (University of Basel, Switzerland) and Dr. C.T. Williams (The Natural History Museum, London) who provide expertise in the mineralogy, petrology, and EPMA analysis of natural zirconolite.

5.4.1 Zirconolite Occurrence and Conditions of Formation

A general list of zirconolite occurrences, host rocks, and associated minerals is given in Table 5.4.1. It is evident that zirconolite formed in silica-undersaturated rocks, i.e., quartz does not appear in the list of associated minerals. This observation indicates that the activity of silica, a_{SiO_2}, is one of the major parameters controlling the stability and survival of zirconolite in nature. As shown in Table 5.4.1, zirconolite is commonly associated with either sphene or perovskite, two indicators of silica activity in rocks. The sphene or perovskite signify moderate or low values of a_{SiO_2}, respectively. Similar relationships can be inferred from the presence of baddeleyite and/or zircon and estimates of a_{SiO_2} can be obtained from the stability fields of these minerals as functions of temperature and pressure. Additional information can usually be obtained from ferrous-ferric mineral associations on the prevailing oxygen fugacity (f_{O_2}) during crystallisation. Moreover if a fluid phase were present, there are other phase assemblages that can be used to estimate its mole fraction of carbon dioxide (X_{CO_2}) in the fluid phase.

The major terrestrial host rocks for zirconolite are syenites, nepheline syenites, carbonatites, and metasomatic rocks. The first three of these are igneous rocks emplaced at

medium to shallow levels in the crust (e.g., depths of < 5-6 up to 10-12 km, equivalent to pressures of < 2 to 4 kbar). Although petrological studies of specific zirconolite bearing igneous rocks are lacking, magnetite-ilmenite equilibria studied by Haggerty[25] indicates that most syenites equilibrated at T = 600-900 °C and log f_{O_2} = -20 to -14 bar. The ubiquitous presence of sphene and absence of quartz in these rocks can be used to estimate their silica activity range (based on sphene-perovskite stability and quartz saturation curves) showing that log a_{SiO_2} = -0.3 to -1.7. For carbonatites magnetite-ilmenite data and other phase equilibria studies likewise indicate equilibration at T = 560-710 °C and log f_{O_2} = -24 to -17 bar [25]. The common occurrence of perovskite in carbonatite rocks places an upper limit on silica activity and is consistent with log a_{SiO_2} < -1.2 to -1.8 at the stated temperatures. Some specific information is available for zirconolite bearing metasomatic rocks. For example, the calcsilicate marble at Bergell, Switzerland probably formed at T > 520 °C and P = 3 kbar (Gieré26). Detailed studies of the zirconolite bearing hydrothermal veins at Adamello, Italy, indicates formation at T = 500-600 °C, P ~ 2 kbar, log f_{O_2} ~ -20 bar, X_{CO_2} ~ 0.2, and log a_{SiO_2} ~ -1 [27],[24]. Further studies of selected localities and mineral assemblages should enable more definitive conclusions to be drawn on the conditions of formation of zirconolite

5.4.2 Crystal Chemistry

The chemical composition of natural zirconolite is extremely complicated; for example, a "complete" analysis by wavelength dispersive electron microprobe (EPMA) or energy dispersive analytical electron microscopy (AEM) involves the determination of 25 elements. However, with the aid of statistical analysis it is often possible to derive a number of simple or coupled substitutions that describe the chemical variation. Knowledge of substitution mechanisms provides information on 1) the solubility limits of REEs, Th, and U in the zirconolite structure, 2) the site occupancies of the REEs, Th, and U together with the identity of important elements involved in coupled substitutions, and 3) the compositional ranges of zirconolite polytypes. These results are important because many of the host rocks have crystallised slowly over long periods of time under geologic conditions that approach chemical equilibrium.

Previous work[28] on the natural zirconolite suite from Bergell, Switzerland indicated a strong positive correlation of Fe^{3+} at the Ti-sites (M5,6) with REEs at the Ca-site (M8). Subsequent statistical analysis of both EPMA and AEM data (Figure 5.4.1) showed that the chemical variations are the result of coupled substitutions of the form:

$$^{M8}Ca + {}^{M5,6}Ti \leftrightarrow {}^{M8}REE + {}^{M5,6}(Al, Fe^{3+}) \quad (1)$$

$$^{M8}Ca + {}^{M5,6}Ti \leftrightarrow {}^{M8}(Th, U) + {}^{M5,6}(Mg, Fe^{2+}). \quad (2)$$

Substitutions (1) and (2) operate simultaneously in the Bergell zirconolites and a least squares fit of REEs vs Th+U gave a slope of 2.4, providing an estimate of the relative magnitude of the two substitutions[29]. Up to 0.4 REE and 0.12 Th+U atoms per formula unit are incorporated at the Ca-site according to substitutions (1) and (2), respectively. A second group of zirconolites from Adamello, Italy, were analysed in detail by Gieré and Williams [24] who found evidence for substitutions (1) and (2) and one additional coupled substitution:

$$^{M8}Ca + {}^{M5,6}Ti_2 \leftrightarrow {}^{M8}REE + {}^{M5,6}Fe^{2+} + {}^{M5,6}(Nb, Ta). \quad (3)$$

In the Adamello zirconolites, REEs are incorporated at the Ca-site by substitution (1) up to ~ 0.1 atoms per formula unit and by substitution (3) at concentrations up to 0.4 atoms per formula unit (Figure 5.4.1). In zirconolites formed at high temperatures in rocks from the Vestfold Hills, Antarctica, Harley[30] presented evidence for a coupled substitution of the form:

$$^{M8}Ca_2 + {}^{M5,6}Ti \leftrightarrow {}^{M8}REE_2 + {}^{M5,6}(Mg, Fe^{2+}). \quad (4)$$

In most natural zirconolites the Zr-site (M7) is essentially fully occupied by Zr and small amounts of Hf. However, site totals vary between approximately 0.9 and 1.1 atoms per formula unit. Much of this variation is statistically significant and can be attributed to the simple substitutions $^{M7}Ti \leftrightarrow {}^{M7}Zr$ (5) and $^{M5,6}Zr \leftrightarrow {}^{M5,6}Ti$ (6). Moreover there is some evidence in the Bergell zirconolite suite for the pyrochlore type coupled substitution:

$$^{M8}Ca + {}^{M7}Zr \leftrightarrow {}^{M8}REE + {}^{M7}REE. \quad (7)$$

The maximum extent of REE incorporation by this mechanism is approximately 0.1-0.2 atoms per formula unit.

A detailed analysis of the crystal chemistry of zirconolite is in progress based on chemical and EPMA analyses from the literature together with our new EPMA data on samples from syenites, nepheline syenites, and carbonatites. The data set now comprise 322 analyses representing 53 individual zirconolite occurrences and 9 different rock types (Table 5.4.1). Theoretical analysis has established that there are 13 important zirconolite end-members and 31 simple and coupled substitution mechanism. In addition to the substitutions listed above, statistical analyses of the EPMA data provide evidence for the following coupled substitutions:

$$^{M5,6}Ti_2 \leftrightarrow {}^{M5,6}(Nb, Ta) + {}^{M5,6}(Al, Fe^{3+}) \quad (8)$$

$$^{M5,6}Ti + {}^{M5,6}(Al, Fe^{3+}) \leftrightarrow {}^{M5,6}(Nb, Ta) + {}^{M5,6}(Mg, Fe^{2+}) \quad (9)$$

$$^{M8}REE + {}^{M5,6}(Al, Fe^{3+}) \leftrightarrow {}^{M8}(Th, U) + {}^{M5,6}(Mg, Fe^{2+}) \quad (10)$$

$$^{M8}Ca + {}^{M5,6}(Nb, Ta) + {}^{M5,6}(Al, Fe^{3+}) \leftrightarrow {}^{M8}(Th, U) + {}^{M5,6}Ti + {}^{M5,6}(Mg, Fe^{2+}) \quad (11)$$

$$^{M8}REE + {}^{M5,6}Ti \leftrightarrow {}^{M8}Ca + {}^{M5,6}(Nb, Ta). \quad (12)$$

Although there are many possible substitution mechanisms, the chemical variation of natural zirconolites is dominated by only a few. These major substitutions are related to the rock-fluid geochemistry and possibly to the oxygen fugacity during crystallisation (Fe^{2+}/Fe^{3+} ratio). Of the twelve substitutions listed above, the most important are (1), (2), (8), (9), and (12). Further refinement of the data set will include an overview of zirconolite chemistry, a description of selected examples from different rock types, and a discussion of the factors controlling the crystal chemistry of zirconolite (e.g., structure, bond strength, crystal field effects, etc.).

The polytypism of zirconolite samples from three localities (Bergell, Kaiserstuhl, and Stavern) have been determined by electron diffraction and in each case, we have found that the crystals are either perfect 2M zirconolite or predominantly 2M with some twinning and stacking disorder. The presence of twinning and stacking disorder in the Bergell samples appears to correlate with increasing amounts of REEs, Th, and U according to substitutions (1) and (2), in agreement with White's[31] work on synthetic zirconolites. Samples from Kaiserstuhl, Germany and Stavern, Norway are also mainly 2M zirconolite with some grains showing evidence of twinning and stacking disorder. Both of these samples are rich in Fe and Nb and also contain REEs, Th, and U, indicating that in natural zirconolites the 2M polytype is not restricted to compositions near the $CaZrTi_2O_7$ end-member. Although it is still possible that one or more key elements are responsible for twinning and stacking disorder, this work suggests that the 2M polytype may be the stable structural configuration for a range of compositions and that other factors in addition to composition may cause twinning and stacking disorder in zirconolite.

5.4.3 Geochemical Alteration

From a geochemical perspective, most of the available evidence indicates that zirconolite is a highly durable phase in both hydrothermal and near surface environments. As an example of the latter case, the zirconolite samples from Sri Lanka occur in stream gravel deposits and therefore have survived the complete destruction of the host rock by weathering. Using samples from Sri Lanka and other localities, Oversby and Ringwood[32] have demonstrated that zirconolite has remained as a closed system to U, Th, and Pb for up to 550

m.y. This result was obtained in spite of the fact that many of the samples are completely metamict (amorphous) due to α–decay of Th and U originally incorporated at the Ca-site (see Section 5.4.4). Nevertheless, there are a few environments in which zirconolite has been destabilised, Gieré and Williams [24] reported corrosion of Adamello zirconolite in a specific mineralogical zone of the host rock (see section 5.4.1) by a reducing hydrothermal fluid rich in H_2S, HCl, HF, and P, but relatively poor in CO_2 ($X_{CO2} \sim 0.2$). Furthermore, in a different and chronologically younger zone of the host rock where the zirconolites normally exhibit little evidence of corrosion [24], we have discovered the mineral betafite. In many cases, the betafite grains appear to be replacing earlier zirconolite grains.

Preliminary results have also been presented which describe the alteration of ~ 2.5 b.y. old zirconolites from Phalaborwa, South Africa[33]. In these samples, the alteration follows microfractures that may have been caused by radiation damaged induced volume expansion of the metamict zirconolites. The chemical pattern of alteration involves incorporation of Si and loss of Ti, Ca, and Fe coupled with hydration (~ 6-12 wt% H_2O, by difference). Much of this Ti and Fe was deposited locally within microfractures, usually as the mineral ilmenite. Minor fluctuation of Zr and REEs also occurs, but the Th and U contents remain relatively constant. Radiogenic Pb, however, appears to have been transiently mobile but was re-precipitated mainly within the altered areas as galena (PbS). Although an estimate of the conditions under which the alteration occurred is not yet available, the mineralogy and analytical results indicate that the fluid phase was rich in Si and S species and poor in Ca and CO_2 (e.g., Ca was removed from the system and no calcite was precipitated as an alteration phase).

Geochemical alteration has been found in three other zirconolite samples. The chemical pattern of patchy alteration (in samples in zirconolite from Langesundfjord, Norway) is similar to that of its Phalaborwa counterpart, with increased Si and H_2O and decreased amounts of Ca and Fe in the altered areas. In samples from Sebl-yavr, Russia, zirconolite is replaced by an unidentified Ba, Ti, Nb, Zr silicate phase, H_2O is enhanced and Ca and Fe are lost. Patchy replacement of zirconolite by an unidentified Ti, Zr, REE silicate phase was also observed in samples from the Cummins Range, Western Australia. All of the above observations point to the instability of zirconolite in the presence of Si-rich fluids under certain as yet unknown P-T conditions, consistent with the information presented in Section 5.4.1 on associated minerals and silica activity. The survival of zirconolite in weathering environments (see Table 5.4.1) suggests that its durability at moderate to low temperatures (e.g., < 300 °C) may reflect kinetic factors.

Natural analogue studies further emphasise the superior performance of zirconolite as compared to other potential actinide host phases including perovskite, zircon, and pyrochlore group minerals. Although zircon, and pyrochlore are durable in hydrothermal fluids and commonly survive the complete destruction of their host rocks by weathering, retaining

actinides in the process, and reports of the alteration of zircon are rare indeed. However, corrosion of zircon is known to occur in metamorphic rocks under hydrothermal conditions similar to those experienced by the Adamello zirconolites, e.g., T ~ 600 °C and elevated HF in the fluid phase[34]. Pyrochlore appears to be more resistant to corrosion by hydrothermal fluids rich in HF, but is subject to alteration via ion exchange and leaching in relatively acidic fluids poor in HF, Ca, and Na[35],[36]. Furthermore, recent work has shown that the Ti-rich member of the pyrochlore group, betafite, may break down to a new phase assemblage in low temperature environments, in some cases resulting in the loss of U[37]. In contrast, field observations indicate that perovskite rarely survives the complete destruction of its host rock by weathering and is usually completely altered to anatase[38]. (Exceptions are found in some rocks where the perovskite contains substantial amounts of Nb and Fe at the Ti-site and the crystals survive weathering, partially altered to anatase (e.g., Erickson and Blade[39]).

5.4.4 Radiation Damage

Due to the incorporation of ^{232}Th, ^{235}U, and ^{238}U atoms at the Ca-site (minor amounts of U may also occupy the Zr-site), natural zirconolites experience α–decay doses of 10^{13} to 10^{18} α/mg depending upon the age of the sample and the amounts of Th and U present. Previous work has shown that α–decay damage causes a crystalline to amorphous transformation in natural zirconolite[40],[41] but an accurate assessment of the dose required to cause the transformation has never been made. Our work has focussed on the use of AEM to accurately measure the Th and U contents of zirconolite, calculate the α–decay dose and dpa, and correlate the results with electron diffraction, bright field, dark field, and high resolution imaging. Preliminary AEM results for samples ranging in age from 16 to 300 m.y. place the transformation zone between ~ 0.08×10^{16} and $1\text{-}2 \times 10^{16}$ α/mg, equivalent to 0.06-1.5 dpa. There is some evidence that the critical dose for amorphisation increases as a function of the age of the samples, consistent with a model of long-term annealing of α–recoil collision cascades back to the original crystalline structure (Lumpkin et al.[41]). The calculated annealing rate constant is approximately $0.4\text{-}1.0 \times 10^{-9}$ yr^{-1} based on a limited set of dose-age data.

Further refinement of the transformation zone and annealing rate constants will be possible on completion of the AEM work on additional samples, most of which have geologic ages of 100 m.y. up to ~ 2.5 b.y. The available data for zirconolite indicate that the dose range of the transformation zone is nearly identical to that of natural zircon[42],[43]. Similar studies of natural pyrochlore suggest that it has a somewhat broader transformation zone and faster annealing rate than zirconolite and zircon[44]. This result is interesting in view of the fact that pyrochlore and zirconolite are both derivatives of the fluorite structure type. At present, the difference in behaviour is poorly understood, but may be related to the closer structural

similarities of pyrochlore and fluorite (a simple ionic structure type that does not become metamict, despite high α–decay doses, e.g., uraninite and thorianite). In general, however, α–decay damage produces similar progressive degradation of crystallinity in zirconolite, zircon, and pyrochlore.

A detailed AEM study of zirconolites from Bergell and Adamello is in progress. Figure 5.4.2 summarises the Th and U contents of the samples and shows that α–decay dose in the grains studied by AEM ranges from ~ 0.01 to 1.1 x 10^{16} α/mg, covering the expected crystalline to amorphous transformation zone. Preliminary results of this work indicate the following radiation damage sequence: 1) The beginning of the transformation (~ 0.05-0.1 x 10^{16} α/mg) is signalled in TEM images by the appearance of weak mottled diffraction contrast and isolated α–recoil collision cascades. 2) With increasing dose (~ 0.1-0.4 x 10^{16} α/mg), the collision cascades overlap to create larger amorphous domains. These domains lead to strong mottled diffraction contrast in TEM images, the appearance of a diffuse ring in electron diffraction patterns, and diminished zirconolite superlattice diffraction spots. 3) Further increases in α–decay dose (~ 0.4-0.7 x 10^{16} α/mg) lead to an increase in the size and volume density of amorphous domains and the appearance of a second diffuse ring in electron diffraction patterns. 4) As the critical dose for amorphisation is approached (~ 0.7-1.0 x 10^{16} α/mg), the structure consists of isolated crystalline domains in an amorphous matrix. At this stage, electron diffraction patterns exhibit two diffuse rings and diminished fluorite subcell diffraction spots. 5) Beyond the critical amorphisation dose (~ 1-2 x 10^{16} α/mg), all traces of crystallinity are eliminated and electron diffraction patterns consist only of diffuse rings. With the exception of a somewhat higher saturation dose, due to long-term annealing, these results are consistent with accelerated damage testing of synthetic zirconolite doped with ^{238}Pu or ^{244}Cm (e.g., Clinard et al.[13], Weber et al.[45]).

5.4.5 Summary and Recommendations

Previous work and investigations carried out to date at ANSTO demonstrate that natural analogue studies are a viable means of examining the stability, crystal chemistry, geochemical alteration, and radiation damage of zirconolite and other waste form phases. Results of these studies are complementary to short-term laboratory investigations and, in specific instances, are the only means of providing information on long-term behaviour (e.g., α–recoil track annealing) at low temperatures. Although the major projects on the crystal chemistry and radiation damage of zirconolite are nearing completion, the following areas have been identified where further studies would be of potential value: 1) mineralogy, petrology, and geochemistry of zirconolite bearing rocks from selected localities with emphasis on determination of the *PTX* conditions; 2) use of SIMS to determine the stable and radiogenic isotope systematics of altered zirconolites, 3) experimental studies of zirconolite stability in

the system $CaO-ZrO_2-TiO_2-SiO_2 \pm CO_2$ and durability in hydrothermal solutions containing Si, F, etc; 4) determination of the annealing kinetics of radiation damaged zirconolite; and 5) experimental studies of the effect of radiation damage on the dissolution of zirconolite.

Table 5.4.1 Summary of zirconolite-bearing host rocks and associated minerals.

Rock type	Occurrences	Associated minerals
kimberlite	3	calcite, ilmenite, zircon, baddeleyite
ultrabasic	2	apatite, zircon, baddeleyite
gabbro	1	allanite, apatite, biotite, epidote, sphene, zircon
syenite	5	allanite, apatite, epidote, ilmenite, sphene, zircon
nepheline syenite	6	apatite, baddeleyite, hibonite, perovskite, zircon, pseudobrookite
carbonatite	16	apatite, baddeleyite, pyrochlore, perovskite, zircon, clinohumite, magnetite
metasomatic	10	allanite, apatite, betafite, calcite, chlorite, diopside, dolomite, geikielite, ilmenite, sphene, pyrite, pyrrhotite, rutile, spinel, clinohumite
metamorphic	1	enstatite, phlogopite, spinel, sapphirine, zircon
placer	2	baddeleyite, perovskite
Lunar basalt	7	baddeleyite, ilmenite

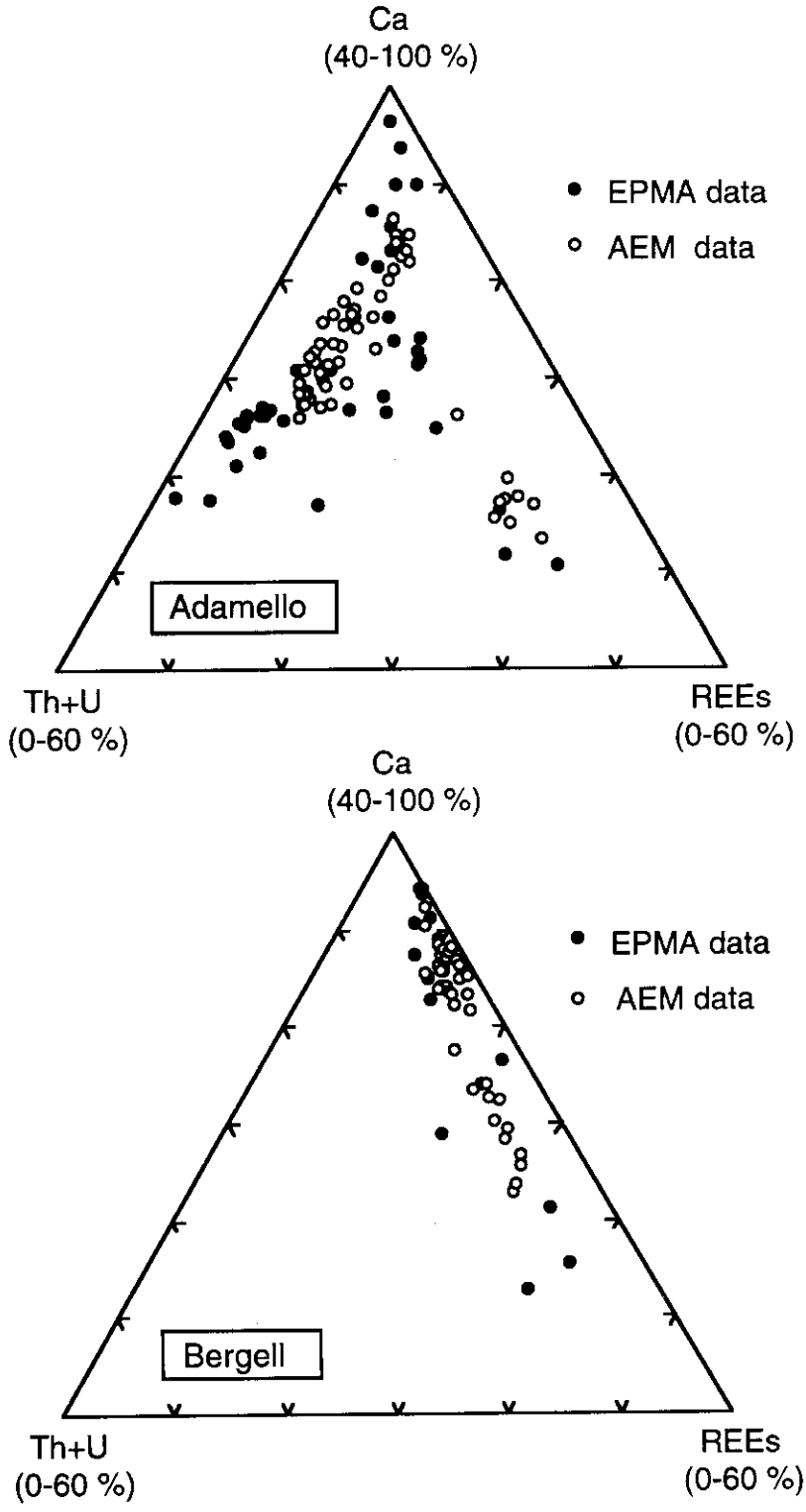

Figure 5.4.1 Triplots showing variation of the major cations at the Ca-site of natural, zoned zirconolites from Adamello, Italy, and Bergell, Switzerland.

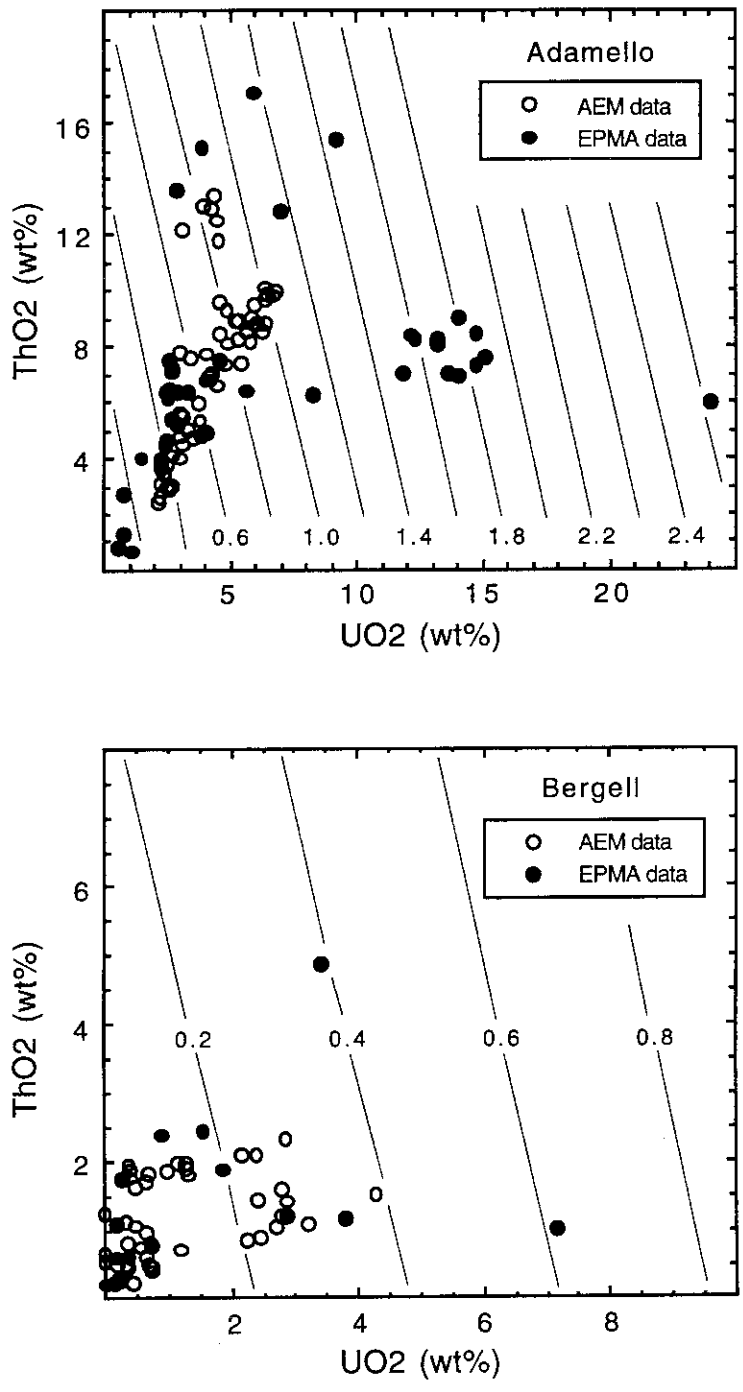

Figure 5.4.2 Plots of the Th and U contents of natural, zoned zirconolites from Adamello, Italy, and Bergell, Switzerland. The plots are contoured for α–decay dose (10^{16} α/mg) based on ages of 42 m.y. for Adamello and 31 m.y. for Bergell.

6. CONCLUSIONS AND RECOMMENDATIONS

6.1 Summary of Work in Phase II

The major activity associated with the Co-operative Program was the preparation, characterisation and subsequent testing of both Cm-doped Synroc containing PW-4b simulated waste and Cm-doped single phase preparations of zirconolite and perovskite, and the initiation of studies on naturally-occurring zirconolites to allow assessment of the long-term durability of this mineral phase over geological time. All of these aspects of the work have been carried out successfully and in particular it has been shown that;

- The Cm-doped reference Synroc (Synroc-C containing simulated PW-4b waste) containing simulated PW-4b waste prepared in the hot-cell facility at JAERI has the expected phase distribution and physical properties. Leach rates of inactive elements from this material are comparable to those prepared in the open laboratory; however, further work is required to determine the effect of Cm-loading on the Cm leach rate.
- Samples of reference Synroc after an equivalent storage age of 13,000 years exhibit Ba and Mo leach rates which are similar to those for 'cold' Synroc samples. Leach rates of Cs are most affected by α–decay damage being a factor of between 5 and 10 higher than that for the 50 year sample. The increase in Ca and Sr leach rates is smaller than that of Cs.
- Cm leach rates from the synroc are unaffected by α–decay damage, and are instead apparently controlled more strongly by the pH of the leachant.
- The density of the Cm-doped reference Synroc decreased linearly with dose and showed no evidence of macro-cracking. Storage of the samples at 200°C reduced the change in density per unit α–dose by a factor of 2 compared to that of the sample stored at room temperature.
- Studies of the Np leach rates of Np-doped Synroc made at ANSTO established that the solution leach rate under oxic conditions was a factor of 10 higher than under anoxic conditions and that the presence of Boom clay (geological host material for the Belgian repository concept) did not markedly affect the leaching behaviour of Np under anoxic conditions.
- Samples of Cm-doped perovskite and zirconolite were prepared but other phases were present in parts of the zirconolite and perovskite specimens. In the extension to the Phase II program there will be a sample and technology interchange program between ANSTO and JAERI to resolve this issue.

- Initial studies of the kinetics and mechanisms of leaching from Synroc have established that releases are not congruent and that future modelling studies will need to include allowances for the effect of hydrated layers on the surface of the specimens on elemental releases.
- Extensive studies were made of crystal-chemical incorporation of rare earths and actinides in zirconolite by XRD and electron microscopy.
- Development of a zirconolite-rich ceramic has reached the stage where good microstructures and very good leaching behaviour of samples containing Nd and U have been obtained.
- Studies of naturally-occurring zirconolites have established that these are viable analogues for the zirconolite phase in Synroc. The major projects on the crystal chemistry and radiation damage of zirconolite have been completed. However, additional work on: mineralogy, petrology, and geochemistry of zirconolite bearing rocks with emphasis on PTX conditions under which the phase has survived; use of SIMS to determine the stable and radiogenic isotope systematics of altered zirconolites; durability studies of zirconolite; determination of the annealing kinetics of radiation-damaged zirconolite and experimental studies of the effect of radiation damage on the dissolution of zirconolite need to be carried out.

The Co-operative Program also involved the establishment of extremely effective collaboration between the staff of the two institutions. This was achieved through personnel exchange and the holding of workshops.

6.2 Conclusions

The second phase of the Co-operative Program has been very successful. It has generated important data which will be of considerable value in evaluating the Synroc process as a means of dealing with HLW and TRU-rich waste streams. The collaboration between the two lead institutions has been particularly good and provides an excellent basis for future work.

The most important scientific conclusions to emerge from the Co-operative Program are:

- Accelerated radiation damage tests on Synroc indicate that there is some deterioration in the leach resistance with increasing equivalent Synroc age.
- Natural samples have confirmed that zirconolite retains actinides over geological time even if subjected to alteration processes as a consequence of contact with hydrothermal fluids.

6.3 Future Work

In the extension to the Phase II program the following work, as identified in this report, should be carried out:

- Studies of the effect of Cm-doping on Cm leach rate from reference Synroc should be carried out at ANSTO.
- A sample and technology exchange program between ANSTO and JAERI on the fabrication of perovskite and zirconolite to obtain single phase specimens followed by a complete characterisation of these phases by both organisations.
- Completion of laboratory-scale studies of actinides in zirconolite, particularly X-ray absorption spectroscopy to examine conclusions form XRD/electron microscopy on Np and Pu valencies.
- Fabrication of laboratory-scale titanate ceramics containing 20 wt% (U,Np,Pu) simulated waste, followed by characterisation via XRD/microscopy, and finally to detailed leach tests.
- Further analogue studies to determine the conditions under which zirconolite survives in the geological environment.
- Development of models to allow the prediction of long-term stability of Synroc and its individual phases under a range of repository conditions.

6.4 Recommendations

The existing, successful program under the Co-operative Agreement should be extended for another three years (from 1995 to 1998) to cover the further description of the performance of Synroc under repository conditions.

APPENDIX 1 SCOPE OF RESPONSIBILITIES OF THE LEAD INSTITUTIONS

ANSTO and JAERI will co-operate in studies on SYNROC for a period of another five (5) years from September 3, 1990 according to the following scope of responsibilities.

JAERI responsibilities

JAERI will continue alpha acceleration test for standard SYNROC and evaluate the performance and capability of SYNROC as a waste form for high-level radioactive wastes.

JAERI will prepare samples of SYNROC containing TRU elements on the basis of hot cell techniques accumulated in JAERI and upon information provided by ANSTO.

JAERI will conduct fundamental research on TRU immobilisation mechanism and study the matrix stability of SYNROC by long-term durability test under the collaboration between ANSTO and JAERI.

JAERI will collaborate in evaluating capability and feasibility of SYNROC system in the high-level waste and TRU waste management based on the results obtained through the co-operative studies described in this Appendix.

ANSTO responsibilities

ANSTO will continue to assess the radiation performance of SYNROC by studies which will include neutron irradiation and natural mineral analogues, and will cooperate with JAERI in the continued evaluation of alpha stability tests.

ANSTO, in collaboration with the Australian National University, will study the formulation, testing and optimisation of SYNROC for immobilisation of TRU elements from the perspectives of waste partitioning, FBR wastes, higher burnup LWR fuel, and other TRU streams.

ANSTO will conduct fundamental research on TRU immobilisation mechanisms, including matrix stability, by structural, leaching and geochemical modeling studies involving SYNROC containing simulated wastes and actinides.

ANSTO will collaborate in evaluating capability and feasibility of the SYNROC system in the high-level waste and TRU waste management based on the results obtained through the cooperative studies described in this Appendix.

APPENDIX 2 MEETINGS OF CO-ORDINATION AND STEERING COMMITTEES

A. Co-ordination Committee Meetings

Meeting No.	Date	Location	Chairman
7	November 22, 1991	Tokyo	H. Ishida
8	November 4, 1992	Canberra	R. Rawson
9	November 3, 1994	Tokyo	T. Kuramochi

B. Steering Committee meetings

Number:	11	Date:	November 22, 1990	Location:	Lucas Heights
Participants:	JAERI	M. Ichikawa			
		S. Muraoka			
	ANSTO	A. Jostsons			
		E. Vance			
		R. Hutchings			
Number:	12	Date:	April 19, 1991	Location:	Tokai
Participants:	JAERI	S. Matsuura			
		M. Ichikawa			
		S. Muraoka			
	ANSTO	A. Jostsons			
	ANU	A. Ringwood			
Number:	13	Date:	November 1, 1991	Location:	Lucas Heights
Participants:	JAERI	M. Ichikawa			
		S. Muraoka			
	ANSTO	A. Jostsons			
		E. Vance			
		R. Hutchings			
	ANU	S. Kesson			
Number:	14	Date:	April 30, 1992	Location:	Tokai
Participants:	JAERI	M. Ichikawa			
		Y. Wadachi			
		S. Muraoka			
	ANSTO	A. Jostsons			
		E. Vance			
		K. Hart			

Number:	15	Date:	November 3, 1992	Location:	Lucas Heights
Participants:	JAERI	M. Ichikawa			
		Y. Kishida			
		S. Muraoka			
	ANSTO	H. Garnett			
		A. Jostsons			
		E. Vance			
Number:	16	Date:	June 11, 1993	Location:	Tokai
Participants:	JAERI	M. Ichikawa			
		Y. Kishida			
		S. Muraoka			
	ANSTO	H. Garnett			
		A. Jostsons			
		E. Vance			
Number:	17	Date:	November 18, 1993	Location:	Lucas Heights
Participants:	JAERI	M. Ichikawa			
		S. Muraoka			
	ANSTO	H. Garnett			
		A. Jostsons			
		E. Vance			
	ANU	S. Kesson			
Number:	18	Date:	May 9, 1994	Location:	ANSTO
Participants:	JAERI	S. Muraoka			
		T. Banba			
	ANSTO	H. Garnett			
		A. Jostsons			
	ANU	S. Kesson			
Number:	19	Date:	November 1, 1994	Location:	Tokyo
Participants:	JAERI	T. Tsujino			
		S. Muraoka			
		T. Banba			
	ANSTO	H. Garnett			
		A. Jostsons			
	ANU	S. Kesson			
Number:	20	Date:	April 28, 1995	Location:	Sydney
Participants:	JAERI	S. Muraoka			
		T. Banba			
	ANSTO	A. Jostsons			
		E. Vance			
	ANU	S. Kesson			

APPENDIX 3 PERSONNEL EXCHANGES

Name: Mr Tamura From: JAERI Visited: ANSTO, Lucas Heights
Date: November 18, 1991 Duration: 3 weeks
Purpose: Liquid analyses and radioanalyses on leachate samples from Synroc.

Name: Dr K. Hart From: ANSTO Visited: JAERI, Tokai
Date: April 10, 1992 Duration: 10 days
Purpose: Preparation of joint publications arising from the co-operative program.

Name: Dr E. Vance From: ANSTO Visited: JAERI, Tokai
Date: April 10, 1992 Duration: 10 days
Purpose: Preparation of joint publications arising from the co-operative program.

Name: Mr Tsuboi From: JAERI Visited: ANSTO, Lucas Heights
Date: November 23, 1992 Duration: 3 weeks
Purpose: Study of the use of XRD technique for the examination of Synroc specimens.

Name: Mr Begg From: ANSTO Visited: JAERI, Tokai
Date: February 8, 1993 Duration: 3 weeks
Purpose: Preparation and characterisation of zirconolite samples.

Name: Dr K. Hart From: ANSTO Visited: JAERI, Tokai
Date: April 27, 1993 Duration: 1 week
Purpose: Preparation of joint publications and scientific discussions on the collaboration.

Name: Dr E. Vance From: ANSTO Visited: JAERI, Tokai
Date: April 27, 1993 Duration: 1 week
Purpose: Preparation of joint publications and scientific discussions on the collaboration.

Name: Mr Kikkawa From: JAERI Visited: ANSTO, Lucas Heights
Date: November 8, 1993 Duration: 3 weeks
Purpose: Study of the fabrication, examination and leaching techniques used at ANSTO for the preparation and characterisation of Synroc.

Name: Mr McGlinn From: ANSTO Visited: JAERI, Tokai
Date: May 11, 1994 Duration: 1 week
Purpose: Study of the leaching of curium-doped perovskite in the hot-cell facilities at JAERI.

Name:	Dr K. Hart	From:	ANSTO	Visited:	JAERI, Tokai
Date:	April 24, 1994	Duration:	1 week		
Purpose:	Discussions on the scientific progress of the collaboration and to initiate the preparation of the phase II report.				

Name:	Mr Numata	From:	JAERI	Visited:	ANSTO, Lucas Heights
Date:	February 6, 1995	Duration:	3 weeks		
Purpose:	Study of the fabrication, examination and leaching techniques used at ANSTO for the preparation and characterisation of actual-sized Synroc.				

APPENDIX 4 WORKSHOPS HELD, DATES, LOCATION AND TOPICS

Workshop

Held at JAERI, Tokai, Japan on October 31, 1994

Participants:	Dr E. Vance	ANSTO
	Dr K. Hart	
	Dr K. Smith	
	Mr P. McGlinn	
	Dr S. Kesson	ANU
	Dr T. Banba	JAERI
	Dr Kamizono	
	Dr Muromura	
	Dr Morita	
	Mr Mitamura	
	Mr Kuramoto	

The main topics discussed at this workshop were;

1. Research and development of HLW partitioning
2. Update on current research on Synroc being carried out at ANSTO
3. New ceramic waste form for disposition of plutonium
4. Natural analogue studies being undertaken within the Synroc program
5. Durability of $La_2Zr_2O_7$ waste form
6. Development of secondary phases on Synroc leached at 150°C
7. Durability of YSZ-Al_2O_3 composite ceramic waste form
8. The effect of pH on the leaching of zirconolite and perovskite
9. α-decay damage of actinide-host phases

APPENDIX 5 LIST OF REFERENCES

1 Japan-Australia Co-operative Program on Research and Development of Technology for the Management of High Level Radioactive Wastes, 1985-1990, Final Report, 1990.

2 Blackford M.G., Smith K.L and Hart K.P., (1992), Proc. Symposium on the Scientific Basis for Nuclear Waste Management XV, Strasbourg, November, 1991, pp 243-249.

3 Smith, K. L., Blackford, M. G., Lumpkin, G.R., Hart, K. P. and Robinson, B. J. (1995) accepted for presentation at Scientific Basis for Nuclear Waste Management XVIX, Boston, USA, November, 1995.

4 Hart, K. P., Robinson, B.J., Payne, T. E., Van Iseghem, P. and Lemmens, K. (1994), Proc. Scientific Basis for Nuclear Waste Management XVIII, Kyoto, Japan, November, 1994, pp 841-845.

5 Vernaz, E., Loida, A., Malow, G., Marples, J. A. C. and Matzke, H., Long-term stability of High-level Wasteforms, presented at the 3rd European conference on Radioactive Waste Management and Disposal, Luxembourg, September 17-21, 1990.

6 Fielding, P.E., and White T.J. (1987), J. Mater. Res. 2, 387-414.

7 K.L. Smith and G.R. Lumpkin, in J.N. Boland and J.D. Fitz Gerald (eds), "Defects and processes in the solid state: Geoscience applications. The McLaren Volume",. Elsevier, Science Publisher B. V., 1993, p401.

8 Kesson, S.E., Sinclair, W.J. and Ringwood, A.E., (1983), Nucl. Chem. Waste Manage, 4, 259-66.

9 Vance, E.R., and Agrawal, D.K., (1982), Nucl. Chem. Waste Manage 3, 229-34.

10 F.W. Clinard, Jr., L.W. Hobbs, C.C. Land, D.E. Peterson, D.L. Rohr, and R.B. Roof, J. Nucl. Mater., 105 (1982) 248 - 256.

11 Clinard, F.W. Jr., Rohr, D.R. and Roof R.B. (1984), Nucl. Instr. Meth. Phys. Res. B1, 581-586.

12 Matzke Hj., Toscano, E., Walker, CT. And Solomah, A.G., (1988), 3, 285-88.

13 Hj. Matzke, I.L.F. Ray, B.W. Seatonberry, H. Thiele, C. Trisoglio, C.T. Walker and T.J. White, J. Amer. Ceram. Soc., 73[2] (1990) 370 - 378.

14 K.L. Smith, G.T. Lumpkin and M.G. Blackford, in C.G. Interrante and R.T. Pabalan (eds.),. Scientific Basis for Nuclear waste Management XVI, Materials Research Society, Pittsburgh, PA, 1993, pp 129 - 136.

15 E.R. Vance, D.J. Cassidy, C.J. Ball and G.J. Thorogood, J. Nucl. Mater., 190 (1992) 295 - 297.

16 Lumpkin, G. R., Smith, K. L. and Blackford, M. G. (1994), Proc. Scientific Basis for Nuclear Waste Management XVIII, Kyoto, Japan, November, 1994, 855-862.

17 Ringwood, A. E., Kesson, S. E., Reeve, K. D., Levins, D. M. and Ramm, E. J.: title. in: Radioactive Waste Forms for the Future, Eds W. Lutze and R. C. Ewing, (1988), 233 - 334.

18 Van Iseghem, P. et al (1995), accepted for presentation at Scientific Basis for Nuclear Waste Management XVIX, Boston, USA, November, 1995.

19 McGlinn, P. J. et al (1994) Proc. Scientific Basis for Nuclear Waste Management XVIII, Kyoto, Japan, November, 1994, pp 847 - 854.

20 D.K. Pham, F.B. Neall, S. Myhra, R.St. C. Smart and P.S. Turner, Scientific Basis for Nuclear Waste management XII (eds. W. Lutze and R.C. Ewing), Materials Research Society, Pittsburgh, PA, USA, p.231, (1989).

21 Levenspiel, O. (1962), Chemical Reaction Engineering; An Introduction to the Design of Chemical Reactors, New York, Wiley.

22 Lumpkin, G.R., Smith, K.L., and Blackford, M.G. (1995) Partitioning of uranium and rare earth elements in Synroc: effect of impurities, metal additive, and waste loading. J. Nucl. Mater. 224, 31-42.

23 Vance, E.R., Begg, B.D., Day, R.A., and Ball, C.J. (1995) Zirconolite-rich ceramics for actinide wastes. Mat. Res. Soc. Symp. Proc., Vol. 353, 767-774.

24 Gieré, R. and Williams, C.T. (1992) REE-bearing minerals in a Ti-rich vein from the Adamello contact aureole (Italy). Contrib. Mineral. Petrol. 112, 83-100.

25 Haggerty, S.E. (1976) Opaque mineral oxides in terrestrial igneous rocks. Reviews in Mineralogy, Vol. 3, 101-300.

26 Gieré, R. (1986) Zirconolite, allanite and hoegbomite in a morble skarn from the Bergell contact aureole: implications for mobility of Ti, Zr and REE. Contrib. Mineral. Petrol. 93, 459-470.

27 Gieré, R. (1990) Quantification of element mobility at a tonalite/dolomite contact (Adamello Massif, Provincia di Trento, Italy). Ph.D. Dissertation, Swiss Federal Institute of Technology, Zürich, 92 p.

28 Williams, C.T. and Gieré, R. (1988) Metasomatic zonation of REE in zirconolite from a marble skarn at the Bergell contact aureole (Switzerland/Italy). Schweiz. Mineral. Petrogr. Mitt. 68, 133-140.

29 Lumpkin, G.R., Smith, K.L., Blackford, M.G., Gieré, R., and Williams, C.T. (1994) Determination of 25 elements in the complex oxide mineral zirconolite by analytical electron microscopy. Micron 25, 581-587.

30 Harley, S.L. (1994) Mg-Al yttrian zirconolite in a partially melted sapphirine granulite, Vestfold Hills, East Antarctica. Mineral. Mag., 58, 259-269.

31 White, T.J. (1984) The microstructure and microchemistry of synthetic zirconolite, zirkelite and related phases. Amer. Mineral. 69, 1156-1172.

32 Oversby, V.M. and Ringwood, A.E. (1981) Lead isotopic studies of zirconolite and perovskite and their implications for long range SYNROC stability. Rad. Waste Manage. 1, 289-307.

33 Lumpkin, G.R., Hart, K.P., McGlinn, P.J., Payne, T.E., Gieré, R., and Williams, C.T. (1994) Retention of actinides in natural pyrochlores and zirconolites. Radiochim. Acta 66/67, 469-474.

34 Wayne, D.M., Sinha, A.K., and Hewitt, D.A. (1992) Differential response of zircon U-Pb isotopic systematics to metamorphism across a lithologic boundary: an example from the Hope Valley Shear Zone, southeastern Massachusetts, USA. Contrib. Mineral. Petrol. 109, 408-420.

35 Lumpkin, G.R. and Ewing, R.C. (1992) Geochemical alteration of pyrochlore group minerals: Microlite subgroup. Amer. Mineral. 77, 179-188.

36 Lumpkin, G.R. and Ewing, R.C. (1995) Geochemical alteration of pyrochlore group minerals: Pyrochlore subgroup. Amer. Mineral. 80, 732-743.

37 Lumpkin, G.R. and Ewing, R.C. (1996) Geochemical alteration of pyrochlore group minerals: Betafite subgroup. Amer. Mineral., in press.

38 Mariano, A.N. (1989) Economic geology of rare earth minerals. Reviews in Mineralogy, Vol. 21, 309-337.

39 Erickson, R.L. and Blade, L.V. (1963) Geochemistry and petrology of the alkalic igneous complex at Magnet Cove, Arkansas. U.S. Geol. Surv. Prof. Paper 425, 95 p.

40 Ewing, R.C. and Headley, T.J. (1983) Alpha-recoil damage in natural zirconolite ($CaZrTi_2O_7$). J. Nucl. Mater. 119, 102-109.

41 Lumpkin, G.R., Ewing, R.C., Chakoumakos, B.C., Greegor, R.B., Lytle, F.W., Foltyn, E.M., Clinard, F.W., Jr., Boatner, L.A., and Abraham, M.M. (1986) Alpha-recoil damage in zirconolite ($CaZrTi_2O_7$). J. Mater. Res. 1, 564-576.

42 Holland, H.D. and Gottfried, D. (1955) The effect of nuclear radiation on the structure of zircon. Acta Crystallogr., 8, 291-300.

43 Murakami, T., Chakoumakos, B.C., Ewing, R.C., Lumpkin, G.R., and Weber, W.J. (1991) Alpha-decay event damage in zircon. Amer. Mineral. 76, 1510-1532.

44 Lumpkin, G.R. and Ewing, R.C. (1988) Alpha-decay damage in minerals of the pyrochlore group. Phys. Chem. Minerals, 16, 2-20.

45 Weber, W.J., Wald, J.W., and Matzke, Hj. (1986) Effects of self-radiation damage in Cm-doped $Gd_2Ti_2O_7$ and $CaZrTi_2O_7$. J. Nucl. Mater. 138, 196-209.

APPENDIX 6 REPORTS AND PUBLICATIONS RESULTING FROM THE JAERI/ANSTO CO-OPERATIVE PROGRAM ON SYNROC

Mitamura, H., Matsumoto, S., Miyazaki, T., White, T. J., Nukaga, K., Togashi, Y., Sagawa, T., Tashiro, S., Levins, D. M. and Kikuchi, A., Self-Irradiation damage of a curium-doped titanate ceramic containing sodium-rich high-level nuclear waste, J. Am. Ceram. Soc. 73[11], 3433–41 (1990).

Hart, K. P., Mitamura, H., Matsumoto, S., Tamura, Y., and Vance, E. R., Immobilisation of actinides and fission products in Synroc"; pp. 976–81 in Proceedings of the Third International Conference on Nuclear Fuel Reprocessing and Waste Management, RECOD'91, Vol. II, Japan Atomic Industrial Forum, Inc., Tokyo, 1991.

Mitamura, H., Matsumoto, S., Hart, K. P., Miyazaki, T., Vance, E. R., Tamura, Y., Togashi, Y., and White, T. J., Aging effects on curium-doped titanate ceramic containing sodium-bearing high-level nuclear waste, J. Am. Ceram. Soc. 75[2], 392–400 (1992).

White, T. J. and Mitamura, H., Quantitative X-ray diffraction analysis of titanate waste forms and its application to damage ingrowth; pp. 109–16 in *Scientific Basis for Nuclear Waste Management Vol. XVI.* Edited by C. G. Interrante and R. T. Pabalan. Materials Research Society, Pittsburgh, PA, 1993.

Mitamura, H., Matsumoto, S., Stewart, M. W. A., Tsuboi, T., Hashimoto, M., Vance, E. R., Hart, K. P., Togashi, Y., Kanazawa, H., Ball, C. J., and White, T. J., Alpha-decay damage effects in curium-doped titanate ceramic containing sodium-free high-level nuclear waste, J. Am. Ceram. Soc. 77[9], 2255–64 (1994).

Muraoka, S. Mitamura, H., Matsumoto, S., Vance, E. R. and Hart, K. P., JAERI/ANSTO Co-operative research on radiation damage and actinide behaviour in Synroc," in Proceedings of 9th Pacific Basin Nuclear Conference, Sydney, 1994.

White, T. J., Mitamura, H., Hojou, K. and Furuno, S., Radiation stability of ceramic waste forms determined by in situ electron microscopy and He Ion irradiation; pp. 227–32 in *Scientific Basis for Nuclear Waste Management* Vol. XVII. Edited by A. Barkatt and R. A. Van Konynenburg. Materials Research Society, Pittsburgh, PA, 1994.

Mitamura, H., Matsumoto, S., Tsuboi, T., Vance, E. R., Begg, B. D. and Hart, K. P., Alpha-decay damage of Cm-doped perovskite; pp. 1405–12 *in Scientific Basis for Nuclear Waste Management* XVIII, Materials Research Society, Pittsburgh, PA, 1995.